

Electronic Thesis and Dissertation Repository

8-18-2020 9:00 AM

Quantifying Mid-pregnancy Placental Metabolism in Guinea Pigs Fed a Lifelong Western Diet

Mary-Ellen E.T Empey, *The University of Western Ontario*

Supervisor: McKenzie, Charles A., *The University of Western Ontario*

A thesis submitted in partial fulfillment of the requirements for the Master of Science degree in Medical Biophysics

© Mary-Ellen E.T Empey 2020

Follow this and additional works at: <https://ir.lib.uwo.ca/etd>



Part of the [Other Medicine and Health Sciences Commons](#)

Recommended Citation

Empey, Mary-Ellen E.T, "Quantifying Mid-pregnancy Placental Metabolism in Guinea Pigs Fed a Lifelong Western Diet" (2020). *Electronic Thesis and Dissertation Repository*. 7177.
<https://ir.lib.uwo.ca/etd/7177>

This Dissertation/Thesis is brought to you for free and open access by Scholarship@Western. It has been accepted for inclusion in Electronic Thesis and Dissertation Repository by an authorized administrator of Scholarship@Western. For more information, please contact wlsadmin@uwo.ca.

Abstract

Maternal consumption of a Western diet (WD) has been linked to alterations in fetoplacental metabolic programming and risk for the exposed fetus to develop obesity, cardiovascular disease, and type II diabetes mellitus. It may also cause oxidative damage to the placental mitochondria. This thesis investigated the metabolic effects of a WD on placentae using a guinea pig model of pregnancy and hyperpolarized ^{13}C MRI for metabolic quantification. It was hypothesized that placental glycolytic metabolism would increase, and placental oxidative metabolism would decrease in WD-fed sows. Control diet- and WD-fed, pregnant sows underwent metabolic MRI at 33 days gestation and were investigated by quantifying the placental lactate-, alanine-, and bicarbonate-to-pyruvate ratios. A statistically significant relationship was detected between placental appearance and metabolism that could be useful as a biomarker of fetoplacental health. These results reinforce the importance of placental metabolic research to determine the relationship between WD consumption and placental metabolism.

Keywords

Pregnancy, placenta, Western diet, metabolism, MRI, hyperpolarized ^{13}C MRI, carbon-13, ^{13}C pyruvate

Summary for Lay Audience

This thesis investigated the effects of eating a high-fat, high-sugar diet during pregnancy. This type of diet is known as the Western diet (WD). The placenta is a temporary but critical organ of pregnancy that can be affected by a WD. The placenta supports the baby's growth and development and provides nutrients. Eating a WD has the potential to impact our short- and long-term health negatively. Eating a WD can alter epigenetic mechanisms. These mechanisms influence how our bodies respond to and process the foods we eat. Changes to these mechanisms predispose a person to develop adverse health conditions. Eating a WD exposes the placenta to a toxic environment. This toxic environment may damage cellular structures and mechanisms involved in metabolism. It alters the processes our bodies use to derive energy from food. This study sought to detect these changes early in pregnancy. Early detection of these changes could be useful as a diagnostic tool. A diagnostic tool would be useful for understanding and detecting babies in metabolic distress. It was expected that eating a WD would result in less efficient methods of energy production. This study investigated metabolic changes in the placenta. A guinea pig model of pregnancy was used because guinea pigs have a similar placental structure and function to the human placenta. Guinea pigs were fed either a WD or a control diet. At mid-pregnancy, guinea pigs underwent specialized MRI techniques to measure metabolism and assess the physical characteristics of the placenta. No significant relationship was detected between diet and metabolism. However, a significant relationship was detected between placental characteristics and metabolism, and this relationship may be a useful indicator of a baby's health. Future work should include the collection of extra mid-pregnancy data. Understanding babies in metabolic distress is critical to our short- and long-term health. Future studies need to clarify the relationship between diet and a baby's health.

Co-Authorship Statement

Chapter 2: “Assessing Mid-pregnancy Placental Metabolism and Physical Characteristics in Guinea Pigs Fed a Lifelong Western Diet,” Mary-ellen ET. Empey, Lanette Friesen-Waldner, Lauren Smith, Lindsay E. Morris, Trevor Wade, Paige Allen, Timothy RH. Regnault & Charles A. McKenzie

Mary-ellen ET. Empey was responsible for data collection, analysis, and interpretation and writing the manuscript. Lanette Friesen-Waldner was responsible for animal care, handling, and preparation, and assisted with data collection. Lauren Smith and Lindsey E Morris assisted with data collection. Trevor Wade assisted with data collection. Paige Allen performed statistical analyses. Timothy RH. Regnault was responsible for animal care and helped supervise the data collection and analysis. Charles A. McKenzie supervised the project.

Acknowledgments

I would like to thank the funding source that supported this study, as well as the following people who assisted in making this research possible.

First, I would like to thank my supervisor, Dr. Charles McKenzie, for his support and guidance in carrying out this research. This has been a valuable learning experience, and I am grateful for his mentorship.

I would also like to thank my advisory committee - Drs. Timothy Regnault and Neil Gelman - for their guidance and advice in completing this research.

Next, I would like to thank my co-authors- Lauren Smith, Lindsay Morris, Paige Allen & Drs. Lanette Friesen-Waldner, Trevor Wade, Timothy Regnault & Charles McKenzie for their contributions to this work.

Dr. Trevor Wade for his advice and technical assistance.

Dr. Lanette Friesen-Waldner for her support, advice, and provision of animal care and preparation.

In addition, I would like to thank my laboratory mates- Stephanie Giza, Simran Sethi, Lauren Smith & Lindsay Morris for their support, advice, and collaboration.

Finally, I would like to thank the National Institutes of Health for funding this research.

Table of Contents

Abstract.....	ii
Summary for Lay Audience.....	iii
Co-Authorship Statement.....	iv
Acknowledgments.....	v
Table of Contents.....	vi
List of Tables.....	ix
List of Figures.....	x
List of Appendices.....	xii
List of Abbreviations.....	xiii
Chapter 1.....	1
1 Introduction.....	1
1.1 Pregnancy.....	1
1.1.1 Placenta.....	2
1.1.2 Uncomplicated vs. Complicated Pregnancies.....	6
1.1.3 Common Complications in Pregnancy.....	7
1.1.4 Importance of Environmental Exposures During Pregnancy.....	9
1.2 Metabolism.....	10
1.2.1 Metabolic Pathways.....	11
1.3 Metabolic Programming.....	14
1.3.1 Cardiovascular Disease (CVD).....	15
1.3.2 Type II Diabetes Mellitus (Type II DM).....	15
1.4 Obesity.....	16
1.4.1 Obesity and Pregnancy.....	17
1.5 Western Diet.....	18

1.5.1	Western Diet for an Animal Model of Pregnancy	19
1.6	Guinea Pig (GP) Model of Pregnancy	19
1.6.1	Western Diet Association	21
1.7	Current Monitoring Methods of Fetoplacental Health.....	21
1.7.1	Diagnostic Medical Ultrasound	21
1.7.2	Fetoplacental Diagnostic Medical Ultrasound Assessment.....	22
1.7.3	Magnetic Resonance Imaging.....	23
1.8	Objective and Hypothesis	28
Chapter 2	29
2	Assessing Mid-pregnancy Placental Metabolism and Physical Characteristics in Guinea Pigs Fed a Lifelong Western Diet.....	29
2.1	Introduction.....	29
2.2	Methods.....	30
2.2.1	Guinea Pig Model of Pregnancy	30
2.2.2	Image Collection.....	31
2.2.3	Hyperpolarized Injection	34
2.2.4	Analysis.....	35
2.3	Results.....	39
2.3.1	Metabolite Production.....	39
2.3.2	Placental Score.....	42
2.3.3	Placental Volume	45
2.3.4	Litter Size.....	46
2.3.5	Pregnancy Loss Rate.....	47
2.3.6	Incidence of Abnormality	48
2.4	Discussion.....	49
2.4.1	Metabolite Production.....	49

2.4.2	Placental Characteristics and Score	50
2.4.3	Placental Volume	53
2.4.4	Litter Size	53
2.4.5	Pregnancy Loss Rate	53
2.4.6	Incidence of Abnormality	54
2.5	Conclusions	54
Chapter 3	55
3	Future Work and Summary	55
3.1	Future Work	55
3.2	Summary	56
References	59
Appendices	66
Curriculum Vitae	68

List of Tables

Table 1: Comparison between ^1H and ^{13}C natural abundance, gyromagnetic ratio, and relative signal strength.	25
Table 2: Summary of T_1 -weighted imaging parameters.	32
Table 3: Summary of the imaging parameters for the BB IDEAL images.	33
Table 4: Summary of hybrid flip angle scheme for metabolic image acquisition.	34
Table 5: Summary of placental characteristics and scoring method.	37
Table 6: Summary of p-values for nested ANOVA statistical analyses. The titled columns represent contributing factors. The titled rows represent factors analyzed as dependent variables. * represents a statistically significant p-value.	40
Table 7: Summary of the mean and standard deviation for the placental LPR, APR, and BPR.	40
Table 8: Summary of the mean litter size data at the time of MRI.	47
Table 9: Summary of mean litter size data at the time of tissue collection.	47
Table 10: Summary of loss rate data.	48
Table 11: Summary of the incidence of placental abnormality data.	48

List of Figures

Figure 1: The placenta (figure adapted [6, 7]). The umbilical cord is seen inserting into the placenta. The chorionic plate is seen on the fetal side, and the basal plate is seen on the maternal side of the placenta.....	3
Figure 2: Placentation [8, 9]. The chorionic villi are seen deep to the chorion, surrounded by the intervillous spaces and bathed in maternal blood for the exchange of nutrients, gases, and waste.	4
Figure 3: The uterus (figure adapted [16, 17]). The uterine cavity, fundus, body, and cervix are demonstrated in this figure.....	6
Figure 4: Metabolic Pathways of Pyruvate [32]. Pyruvate can be converted to alanine or lactate in the cytoplasm, or it can enter the mitochondria and produce bicarbonate as a by-product of aerobic cellular respiration pathways. The ¹³ C ₁ label is indicated on pyruvate and its metabolites and by-products.	14
Figure 5: This figure demonstrates the percentage composition of carbohydrates, fats, and protein in the control and Western diets [7, 45].....	19
Figure 6: A-C. This figure demonstrates the distribution of the LPR (A), APR (B), and BPR (C) data in CD- and WD-exposed placentae. No statistically significant relationships were detected using a Nested ANOVA. Data points coded with the same colour within a diet group are part of the same litter.	41
Figure 7: A-C. This figure represents the distribution of LPR (A), APR (B), and BPR (C) data across placental score. Data points coded with the same colour are part of the same litter. Statistically significant variation was detected for the APR (B) and BPR (C), but not for the LPR (A) using a Nested ANOVA.....	42
Figure 8: This figure demonstrates the distribution of the placental score data between CD- and WD-exposed placentae. No statistically significant relationships were detected using a	

Nested ANOVA. Data points coded with the same colour within a diet group are part of the same litter..... 43

Figure 9: A-F. T₁-weighted images. A: demonstrates normal placentae. The white arrows indicate normal-appearing placentae. B: demonstrates characteristics i and ii from Table 5. The white arrow indicates a poorly visualized placenta. The black arrow indicates a poorly differentiated placental border. C: demonstrates characteristic iii from Table 5. The white arrow indicates the location of the placenta. The black arrows indicate an irregular placental border. D: demonstrates characteristic iv from Table 5. The white arrow indicates the location of the placenta. The black arrow indicates an area of heterogeneity with increased signal intensity relative to the rest of the placenta. E: demonstrates characteristic v from Table 5. The black arrow indicates the location of the placenta. The white area indicates a hyperintense placental border or "halo." F: demonstrates characteristic vi from Table 5. The white arrow indicates the location of the placenta, and the black arrow indicates a hyperintense placental border. No discernible, associated fetus could be identified in this instance. 44

Figure 10: T₁-w image displaying motion artefact over the maternal abdominopelvic region. The white arrows indicate motion artefact both external to the sow and within the maternal abdominopelvic structures. 45

Figure 11: This figure demonstrates the distribution of the placental volume data between CD- and WD-exposed placentae. No statistically significant relationships were detected using a Nested ANOVA. Data points coded with the same colour within a diet group are part of the same litter..... 46

List of Appendices

Appendix 1: Permission for Figure 4.....	66
Appendix 2: AUP Original Approval.	67
Appendix 3: AUP Renewed Approval.....	67

List of Abbreviations

Abbreviation	Meaning
LMP	Last menstrual period
GA	Gestational age
WD	Western diet
CD	Control diet
GP	Guinea pig
VEGF	Vascular endothelial growth factor
PIGF	Placental growth factor
IUGR	Intrauterine growth restriction
Type II DM	Type II diabetes mellitus
CVD	Cardiovascular disease
DOHaD	Developmental origins of health and disease
NAFLD	Non-alcoholic fatty liver disease
NASH	Non-alcoholic steatohepatitis
ATP	Adenosine triphosphate
Acetyl Co-A	Acetyl coenzyme-A
TCA	Tricarboxylic acid
LDH	Lactate dehydrogenase

ALT	Alanine aminotransferase
PDH	Pyruvate dehydrogenase
OXPHOS	Oxidative phosphorylation
IMM	Inner mitochondrial membrane
NADH ₂	Nicotinamide adenosine dinucleotide
CO ₂	Carbon dioxide
O ₂	Oxygen
DNA	Deoxyribonucleic acid
MRI	Magnetic resonance imaging
BMI	Body mass index
CRL	Crown-rump length
AC	Abdominal circumference
BPD	Biparietal diameter
AFI	Amniotic fluid index
FL	Femur length
FHR	Fetal heart rate
MCA	Middle cerebral artery
FID	Free induction decay
B-mode	Brightness-mode
RF	Radio-frequency

DNP	Dynamic nuclear polarization
FA	Flip angle
BB IDEAL	Broadband iterative decomposition of water and fat with echo asymmetry least-squares estimation
PD	Proton density
DWI	Diffusion-weighted imaging
AUC	Area under the curve
HFA	Hybrid flip angle
k_{PL}	Rate constant of conversion: pyruvate to lactate
k_{PA}	Rate constant of conversion: pyruvate to alanine
k_{PB}	Rate constant of conversion: pyruvate to bicarbonate
LPR	Lactate-to-pyruvate ratio
APR	Alanine-to-pyruvate ratio
BPR	Bicarbonate-to-pyruvate ratio
SPGR	Spoiled gradient-echo sequence
SI	Signal intensity
ROS	Reactive oxygen species
TR	Repetition time
TE	Echo time
FOV	Field of view

B_0	Main magnetic field
B_1	Radio-frequency magnetic field
^{13}C	Carbon-13
^{12}C	Carbon-12
C_1	Label on carbon #1
C_2	Label on carbon #2
^1H	Hydrogen
$T_1\text{-w}$	T_1 -weighted
$T_2\text{-w}$	T_2 -weighted
T_1	Longitudinal relaxation
T_2	Transverse relaxation
T	Tesla
K	Kelvin
kg	Kilograms
kg/m^2	Kilograms/square metre
mg/kg	Milligrams/kilogram
L/min	Litres/minute
MHz	Megahertz
s	Seconds
ms	Milliseconds

mm	Millimetres
mL	Millilitres
cm	Centimetres
cc	Cubic centimetres
*	Statistically significant result

Chapter 1

1 Introduction

This thesis introduction begins by describing the normal progression of pregnancy, as well as complications that may be encountered during pregnancy. Next, *in utero* environmental exposures and obesity and its effects during pregnancy are examined. Third, this thesis provides background information on the Western diet, metabolic programming, and placental development, role, and metabolism. Additionally, current monitoring methods of fetoplacental health and hyperpolarized magnetic resonance imaging are described. Last, this introduction examines analysis methods and animal models.

1.1 Pregnancy

Pregnancy in humans refers to the period during which a fetus develops within a female's uterus. A typical gestational period is approximately 40 weeks and is measured from the first day of the last menstrual period (LMP) to delivery. The gestational age (GA) of a fetus refers to the current duration of pregnancy. It is counted from the first day of the last menstrual period. GA is usually expressed in weeks and days, and pregnancy is commonly divided into three trimesters. The first trimester lasts from zero days LMP to the end of the 13th week of pregnancy. This trimester encompasses events such as rapid cell divisions, placentation, and embryonic organogenesis. The first trimester of pregnancy is a critical period of development, during which time the embryo/fetus is particularly sensitive to disruptions in its environment and development. The second trimester lasts from 14 weeks to the end of the 27th week [1]. During this period, we see continued development of the fetal form and function [2] and a fully developed and functioning placenta [1]. The third trimester lasts from the 28th week of pregnancy until delivery. By this time, the fetus is mostly developed and gains weight rapidly [2], attributable primarily to the increasing development of subcutaneous adipose tissue [3]. The placenta, while still supporting the fetus, matures and follows a normal path of decline approaching the delivery of the fetus, which marks the end of pregnancy [1].

1.1.1 Placenta

The placenta is a fetal organ that exists only during pregnancy and acts as an interface between the maternal and fetal environment to support fetal growth and development. Anatomically, the placenta has a “maternal side,” known as the basal plate and a “fetal side,” known as the chorionic plate. The basal plate is formed by the decidua basalis, which is the term given to the layer of decidua that lies deep to the conceptus. The decidua is the term given to the functional layer of endometrium in a gravid uterus [1]. The chorionic plate is composed of the amniochorionic membrane and fetal vessels [4]. The human placenta is known to be hemochorial in structure, meaning that there is a single layer of chorionic cells (syncytiotrophoblasts) separating maternal and fetal circulation of red blood cells [5].

Typically, the placenta is a flattened, circular, metabolically active, highly vascularized and low-resistance organ that weighs approximately 600 grams at term and is 2-4cm thick depending on gestational age. It can attach to the uterine wall anywhere within the uterine cavity, with the maternal side being comprised of nearly 20 functional lobes composed of maternal sinusoids and chorionic villous structures. Generally, the placenta has a homogeneous tissue texture and smooth borders with central insertion of the umbilical cord - the vascular connection between the fetus and placenta.

The retroplacental complex is a 20cm-thick, vascularized zone just deep to (or underneath) the basal plate of the placenta and is composed of decidua basalis, uterine myometrium, and maternal veins, which drain the placenta [1]. The gross placental structure and umbilical cord can be seen in Figure 1.

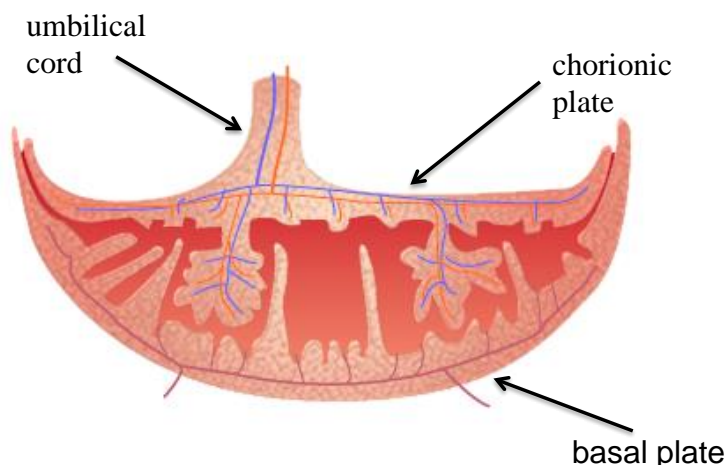


Figure 1: The placenta (figure adapted [6, 7]). The umbilical cord is seen inserting into the placenta. The chorionic plate is seen on the fetal side, and the basal plate is seen on the maternal side of the placenta.

1.1.1.1 Placental Development

The placenta is composed of parenchyma, chorion, amnion, and the umbilical cord. The trophoblast is formed from the trophoblast. Contact between the endometrium and the trophoblast, during implantation of the blastocyst, initiates the development of the syncytiotrophoblast and the cytotrophoblast. The cytotrophoblast secretes enzymes that erode the endometrial cells and allows for invasion of the endometrial wall by syncytiotrophoblast cells [4].

The placenta is formed by the chorion, which is composed of syncytiotrophoblast, cytotrophoblast, and extraembryonic mesoderm. The syncytiotrophoblasts and cytotrophoblasts are specialized placental cells that line the chorionic villi. The cytotrophoblast pushes into the syncytiotrophoblast, forming finger-like projections called the primary chorionic villi. The secondary chorionic villi are formed when the extraembryonic mesoderm divides into splanchnic and somatic mesoderm. The completed formation of blood cells and vessels from mesenchyme marks the presence of tertiary chorionic villi. A vascular network then develops from the villi connecting to the

embryonic heart as the villi continue to grow and branch into the chorion, bathed in maternal blood in the intervillous spaces from remodelled maternal uterine spiral arteries in each of the functional lobes of the placenta. As placental development continues, the amnion and chorion fuse. Together with the fetal vessels, this forms the chorionic plate of the placenta. By the third month of pregnancy, the placenta is fully developed and is functioning to support the developing fetus [4].

1.1.1.2 Role of the Placenta

The placenta is considered to be an immune and endocrine organ that functions to support fetal growth and development by acting as an interface between maternal and fetal environments. The exchange of maternal and fetal substances occurs across the chorionic membrane of the villi and the intervillous spaces containing maternal blood. Oxygen and carbon dioxide, hormones, maternal antibodies, electrolytes, fetal waste, and nutrition for the fetus in the form of amino acids, water, vitamins, free fatty acids, and glucose are exchanged across the membrane [4]. Figure 2 demonstrates placentation.

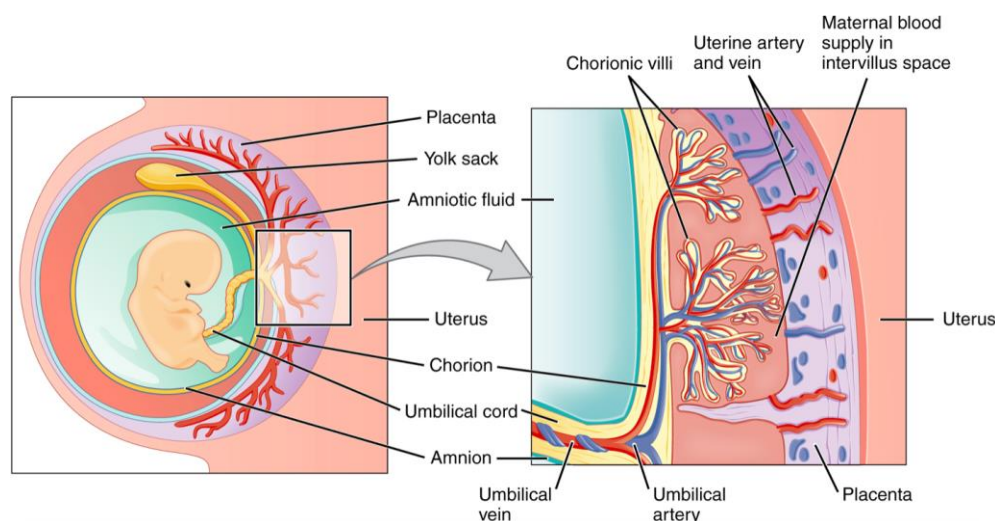


Figure 2: Placentation [8, 9]. The chorionic villi are seen deep to the chorion, surrounded by the intervillous spaces and bathed in maternal blood for the exchange of nutrients, gases, and waste.

1.1.1.3 Placental Metabolism

Metabolically, the placenta serves to produce glycogen (from maternal glucose) and cholesterol (from maternal fatty acids). The cholesterol produced is used to generate

hormones like estrogen, progesterone, and glucocorticoids that help to sustain the pregnancy and influence fetal development [4]. The placenta also synthesizes peptide hormones such as vascular endothelial growth factor (VEGF) and placental growth factor (PIGF), which have a role in placental development and maternal spiral artery remodelling [10]. Glycogen produced in the placenta is stored for use as energy for the fetus [4].

While the placenta provides energy via glycogen storage to the fetus, the placenta itself requires energy from glucose to function. The fetal environment is known to be naturally hypoxic [11], and levels of oxygen in the placenta during the first trimester are also naturally low [12]. In this low-oxygen state, energy for the placenta is derived from the production of lactate through aerobic glycolysis [13].

The presence of an adverse maternal metabolic environment has the potential to alter the normal metabolic processes and efficiency of the placenta. Some studies have shown that a high fat, high sugar maternal environment leads to abnormal accumulation of lipids in the placenta and also suggest that exposure of the placenta to a lipotoxic environment may lead to oxidative damage to placental mitochondria, the cellular organelles responsible for placental metabolism and energy production [14, 15].

1.1.1.4 The Uterus

The uterus is a muscular organ that forms part of the female reproductive system. The uterus is where implantation and growth of a conceptus occurs and plays a significant role in the labour and delivery of a fetus by producing strong muscle contractions that ultimately expel the fetus from the uterus during the birthing process. There are four segments to the uterus - the fundus, the corpus, the isthmus, and the cervix. The uterus contains an internal cavity, which is lined with endometrium - a mucosa, which is the innermost of three uterine layers of tissue. The outermost layer is the serosa, which is thin. The middle layer is the thick, muscular layer called the myometrium [1].

The endometrium is a specialized mucosal tissue that responds to changes in hormone levels throughout the menstrual cycle by altering its thickness and composition to

accommodate and support the implantation of a fragile conceptus. The endometrium has two layers: a superficial functional layer and a deep basal layer. It is the functional layer of the endometrium that is termed the decidua in the gravid uterus. The decidua is further subdivided based on its anatomical relationship to the implanted conceptus. The decidua basalis is deep to the conceptus, and the decidua capsularis overlies the conceptus. Finally, the decidua parietalis refers to all remaining portions of the decidua [1]. Figure 3 demonstrates the anatomy of the uterus.

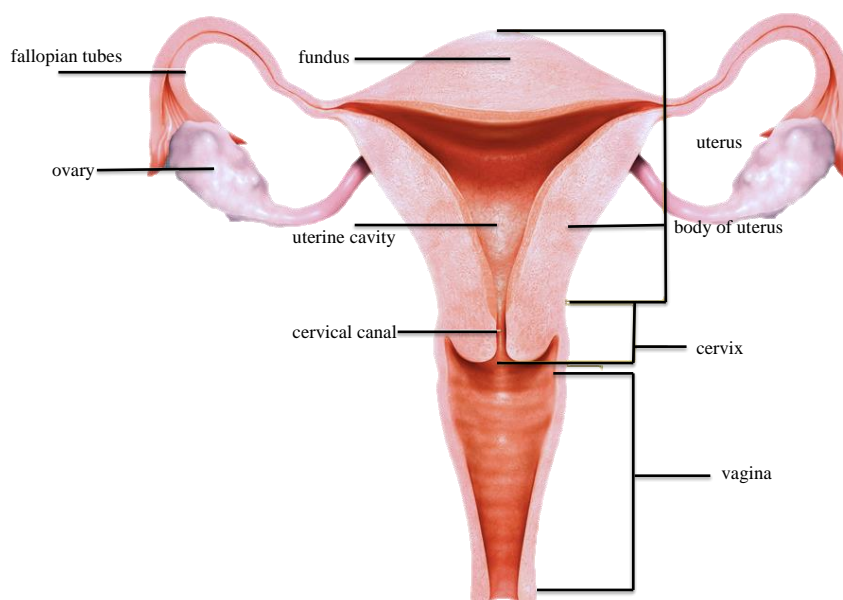


Figure 3: The uterus (figure adapted [16, 17]). The uterine cavity, fundus, body, and cervix are demonstrated in this figure.

1.1.2 Uncomplicated vs. Complicated Pregnancies

Many pregnancies progress without complication, resulting in the uncomplicated births of normally developed and functioning, healthy babies. However, there are many pregnancies plagued by complications relating to maternal health before and during pregnancy. Fetal development and environment, including *in utero* exposures to toxins, viruses, and adverse maternal environment, can also lead to complications in pregnancy. Additional complications may arise during delivery or following delivery in the postnatal period [1].

1.1.3 Common Complications in Pregnancy

During pregnancy, there are many sources for complications, which may arise from maternal and/or fetal health status. Some of the more common or serious complications include maternal and fetal exposures to infectious disease, diabetes mellitus, maternal hypertension, preeclampsia, intrauterine growth restriction (IUGR), preterm labour, and pregnancy miscarriage and stillbirth [18]. Conditions such as diabetes, IUGR, and macrosomia are potentially associated with metabolic dysregulation, which may affect metabolic regulation in the fetoplacental unit.

Infections with the potential to affect the healthy development and outcome of a pregnancy include some sexually transmitted infections and infections such as varicella and rubella [1]. These infections can pass from mother to fetus during pregnancy or can be passed on to the neonate via the birth canal in a vaginal delivery. Some of the consequences of maternal infection during pregnancy are a congenital anomaly in the neonate, low birth weight, miscarriage and stillbirth, and neonatal death. Luckily, many of these infections can be prevented or treated and managed with appropriate medical care before and during pregnancy [1, 18].

Diabetes mellitus, a disorder of carbohydrate metabolism, associated with a deficiency in insulin and characteristic hyperglycemia, can be classified into several types. Some of the more familiar types are type I, type II, and gestational diabetes. Gestational diabetes mellitus only occurs during pregnancy, while other types may occur outside of pregnancy and can persist during pregnancy [1].

Having diabetes mellitus during pregnancy is associated with fetal congenital anomalies in the skeletal, central nervous, cardiac, renal, and gastrointestinal systems and anomalies in the umbilical cord, as well as a 15-20% spontaneous abortion rate. These anomalies are associated with high blood sugar levels, as in hyperglycemia, which disrupts embryonic organogenesis leading to anomalous organ system development. Diabetes mellitus in pregnancy may also lead to abnormal growth conditions such as IUGR and macrosomia.

IUGR is commonly defined as an “estimated fetal weight less than the 10th percentile for the gestational age”, but this is not the only accepted definition. Unfortunately, the existence of several definitions for IUGR contributes to a lack of consistency in diagnosis [1]. Consistency in diagnosis and appropriateness of definitions for the diversity of the population may also be relevant to the definition and diagnosis of macrosomia in light of racial, genetic, and sex differences [19, 20].

Fetuses diagnosed with IUGR have increased risk of perinatal mortality and are more likely across their lifespan to develop conditions such as hypertension, cardiovascular disease, diabetes mellitus, and obesity. Fetal development of IUGR is more prevalent in women with hypertension, and preeclampsia is associated with the most severe growth deficits in terms of maternal factors that may influence fetal growth restriction. IUGR in fetuses of diabetic mothers is attributed to uteroplacental vascular insufficiency in which there is less maternal blood reaching the fetus through the placenta carrying critical nutrients and oxygen needed for normal growth [1].

Macrosomia in a fetus is defined as a fetal weight greater than 4500 grams or a birth weight above the 90th percentile for gestational age. It may result from fetal hyperinsulinemia (excessive insulin), as excessive sugars from maternal hyperglycemia enter the fetal circulatory system through the placenta and stimulate fetal insulin production [21]. Fetal hyperinsulinemia prompts increased growth of body tissues, including adipose tissue. Macrosomic fetuses are predisposed to stillbirth and intrapartum trauma, such as shoulder dystocia [1]. Similar to fetuses with IUGR, macrosomia predisposes a fetus to cardiovascular and metabolic conditions across their lifespan, including diabetes mellitus and obesity [3, 20]. Risk factors for developing fetal macrosomia include maternal diabetes mellitus (type I, II, or gestational), excessive maternal weight gain, and obesity [1].

Maternal hypertension (high blood pressure) is associated with co-morbidities such as diabetes mellitus and obesity [22] and may exist before pregnancy or may develop during pregnancy. If, in addition to hypertension, proteinuria and/or edema develop, we call this toxemia of pregnancy or preeclampsia. Preeclampsia can increase the prenatal mortality

rate and can also develop into the more severe eclampsia involving maternal convulsions and a significant increase in fetal and maternal mortality [1]. Conditions associated with preeclampsia include fetal distress, low birth weight, and placental abruption. While the etiology of preeclampsia is unclear, hormonal, immunologic, and diet-related factors are considered to be contributors to its development. The proposed etiologic factors are likely responsible for the placental vascular disease and reduced uteroplacental blood flow seen in preeclamptic patients, leading to limited oxygen and nutrient delivery to the fetus via the placenta and ultimately leading to unfavourable outcomes [1].

In summary, there are fetal, maternal, and placental factors intimately intertwined with the external and internal maternal environment, including diet, which can lead to a complicated pregnancy.

1.1.4 Importance of Environmental Exposures During Pregnancy

Exposure to toxins and other harmful agents can come from interactions with other people in the form of viruses and bacteria, as well as from polluted air, contaminated water, inhaled or ingested substances, and the foods we consume [1, 23-25]. All of these sources have the potential to negatively impact our health in the short-and long-term, with pregnant women and their fetuses being no exception. *In utero* exposure to these environmental factors can have obvious and disabling effects upon the fetus as in fetal alcohol syndrome that results from alcohol consumption during pregnancy. They can also have silent, insidious effects on the fetus, such as the epigenetic changes to metabolic programming seen with maternal consumption of a poor diet and poor maternal metabolic health [26].

1.1.4.1 Importance of Maternal Environment

The concept of the developmental origins of health and disease (DOHaD) postulates that exposure to some environmental factors during crucial periods of growth and development could have a significant impact on the short- and long-term health of an individual. This concept suggests that when a developing fetus is exposed to an inhospitable uterine environment, caused by insults such as poor nutrition, chemicals, or metabolic and hormonal dysregulation, it responds by developing adaptations to ensure

its survival in the short term, but also its survival should a similar environment arise later in life [27].

The quality of the time a fetus spends *in utero* is critical to its healthy growth and development and the quality of life of the individual across their lifespan. Since the fetus is exposed, through the placenta, to the maternal environment, we must consider the effect that maternal constitutional factors have on the fetus and placenta. Constitutional factors refer to a basic physiological tendency that affects the etiology of specific physical conditions, for example, physiological characteristics relating to circulatory and metabolic function. The maternal diet consumed before and during pregnancy can affect constitutional factors relating to maternal cardiometabolic health. Previous studies have shown that both maternal under and overnutrition can result in altered fetoplacental metabolic programming, perhaps as an adaptive mechanism to prepare for the presumed adverse environment [28] after birth. Some diets, such as the Western diet (WD), are calorie-dense and nutritionally deficient and are associated with the development of overweight and obesity, type II diabetes mellitus (DM), cardiovascular disease, and deposition of excess dietary energy. This excess dietary energy is stored as fat in ectopic and cardiometabolically unhealthy fat storage depots in the body, such as intraabdominal fat stores and intra-organ fat stores (*e.g.* the storage of excess lipid in the hepatocytes of the liver). Previous studies have shown that obesity, diabetes mellitus, and chronic consumption of high fat, high sugar diets, such as the WD, lead to a lipotoxic and hyperglycemic environment with the potential to impact placental development and function negatively, and subsequently impact fetal health and programming outcomes [15, 29].

In summary, the quality of our *in utero* environment can affect our lifetime health and quality-of-life trajectory, beginning with the placenta - the interface between maternal and fetal environments.

1.2 Metabolism

Metabolism refers to the chemical reactions that take place within our bodies to provide our cells with energy, as required, to maintain homeostasis and sustain life [30].

Anabolic metabolism is the generation of larger molecules from smaller subunits, as in the formation of glycogen from glucose for storage of energy. Catabolic metabolism refers to the “breakdown” or oxidation of macronutrients, such as fats and carbohydrates, for the production and use of energy in the form of adenosine triphosphate (ATP) [30].

Energy balance must be reached to achieve homeostasis, meaning that our energy intake from macronutrients must be in balance with the oxidation of those macronutrients.

While fats are a high-energy fuel, our dietary need for them is low, and most dietary fat intake is stored in adipose tissue and not oxidized for use as energy unless energy generation from carbohydrate intake is insufficient to meet daily energy requirements.

Carbohydrates are the primary fuel source for energy production in humans and can be metabolized to a usable form via several pathways, with the fundamental molecular unit being glucose. If the composition of an individual’s diet is changed, metabolic flexibility may allow the body and cells to match the oxidation of fuels to the availability of fuels. Impairment of this metabolic flexibility may lead to increased dietary energy intake to maintain homeostasis. An obese state sees excess glucose converted to triglycerides via lipogenesis and stored in adipocytes. In a state of lipotoxicity, triacylglycerol accumulates in the lipid droplets of hepatocytes, skeletal muscle, and pancreatic beta cells. This accumulation in the lipid droplets is a significant factor in the pathogenesis of insulin resistance, type II DM, and metabolic syndrome [31].

1.2.1 Metabolic Pathways

There are specific metabolic pathways for each type of macronutrient we consume.

Dietary carbohydrates are broken down to glucose in most cases and enter either a non-oxidative or oxidative pathway. The metabolic pathway which will be utilized is determined by the presence or lack of oxygen, type of cells composing the tissue, and the intracellular energy level.

In the presence of oxygen, mitochondria, and a cellular need for energy, glucose oxidation begins with the formation of two pyruvate molecules from a single glucose molecule via glycolysis. Following this, decarboxylation of pyruvate occurs, producing two molecules of acetyl coenzyme A (acetyl-CoA), which can then be used in the

tricarboxylic acid (TCA) cycle. The TCA cycle is also called the citric acid cycle and the Krebs cycle. This decarboxylation process links glycolysis and the TCA cycle. Following the TCA cycle, oxidative phosphorylation occurs, from where the majority of ATP produced via aerobic respiration is derived [30].

In the absence of oxygen, or in cells without mitochondria, the anaerobic respiratory process of glycolysis occurs. Pyruvate is converted to lactate or alanine via enzymatic activity to produce, albeit much less efficiently than aerobic respiratory processes, cellular energy. The process of glycolysis occurs in the cellular cytoplasm. Pyruvate is converted to lactate via the enzyme, lactate dehydrogenase (LDH). Alanine is derived from pyruvate in a transamination process that uses the catalyzing enzyme alanine aminotransferase (ALT).

As mentioned previously, pyruvate can also be converted to acetyl-CoA via the enzyme pyruvate dehydrogenase (PDH) in the PDH reaction, which occurs in the mitochondria. Carbon dioxide (CO_2), a waste product of this reaction, is in equilibrium with cellular bicarbonate. Insulin stimulates this reaction and consequently also stimulates the TCA cycle.

The TCA cycle also occurs within the mitochondria and is a biodegradation process that begins with the joining of oxaloacetate to acetyl-CoA, forming the TCA cycle intermediate, citrate. As the cycle continues, multiple intermediates are generated through enzymatic reactions. The cycle ends where it began with oxaloacetate, having generated high-energy coenzymes and by-products such as CO_2 .

The oxidative phosphorylation (OXPHOS) reaction, occurring in the mitochondria, oxidizes reduced, high-energy coenzymes, such as nicotinamide adenine dinucleotide (NADH_2), via the release of its hydrogen. The energy from hydrogen's electron is slowly transferred to oxygen through a series of enzymatic reactions. These enzymes use the energy released to generate a proton gradient across the inner mitochondrial membrane

(IMM), which ultimately provides the energy for ATP generation. Water and CO₂ are produced as by-products of OXPHOS [30].

Overall, a theoretical 38 ATP molecules are produced from one glucose molecule via cellular respiration. In contrast, glycolysis- whether aerobic or anaerobic, produces only 2 ATP molecules per glucose molecule consumed in the process.

Given that these processes are regulated by factors such as insulin and intracellular energy levels, metabolic conditions that alter these factors can drastically change the pathway for carbohydrate metabolism and also result in changes to the metabolic pathways for other macronutrients, such as fats [30].

Recognizing that placental health is critical to fetal development and that the placenta is a poorly understood organ, it is paramount that we continue to broaden our understanding of placental development and function - including metabolism, particularly in conditions of metabolic dysregulation.

1.2.1.1 Pyruvate

In this thesis, the interest was in the metabolic fate of intravenously injected, supra-physiological concentrations of a hyperpolarized, carbon-13-labelled pyruvate (¹³C-labelled pyruvate) solution (labelled in the C₁ position) for two main reasons. First, understanding that glucose is the primary fuel for our bodies' cells, metabolic pathways for carbohydrate metabolism are of critical importance. As has been outlined, pyruvate is the product of the partial oxidation of glucose during glycolysis, making it an integral component in the process of cellular energy production from glucose. Second, pyruvate's intersection with the LDH reaction, transamination to alanine, and PDH reaction- leading to the TCA cycle, allows for quick, quantitative probing of these pathways [30]. Figure 4 demonstrates the location in the cell where the ¹³C₁-labelled reactions of interest take place.

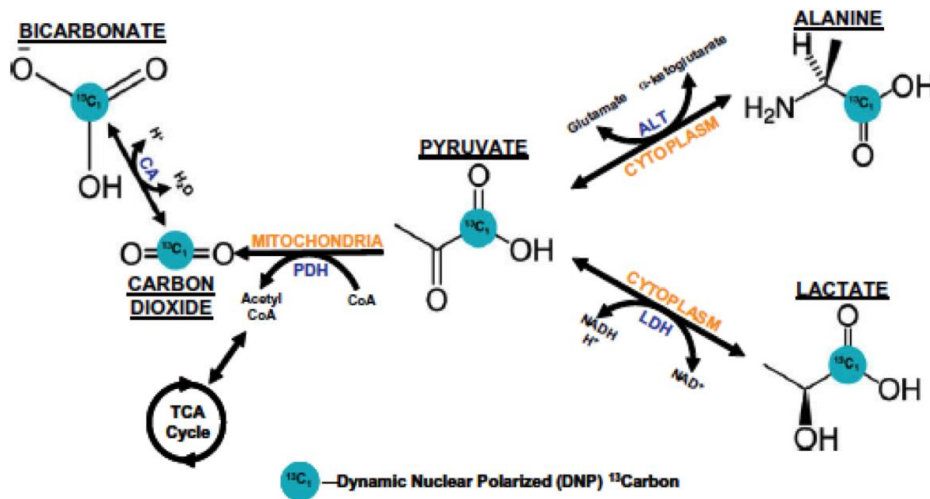


Figure 4: Metabolic Pathways of Pyruvate [32]. Pyruvate can be converted to alanine or lactate in the cytoplasm, or it can enter the mitochondria and produce bicarbonate as a by-product of aerobic cellular respiration pathways. The $^{13}\text{C}_1$ label is indicated on pyruvate and its metabolites and by-products.

1.3 Metabolic Programming

The predisposition of the offspring of diabetic and/or obese mothers to developing cardiometabolic conditions later in life is likely the result of early programming of fetal organ structure and metabolism due to an unfavourable fetal nutritional environment. *In utero* exposure to overnutrition (excess dietary glucose and fat) likely alters early-pregnancy processes like epigenetic changes via DNA methylation, placentation, and fetal organogenesis [28]. These changes result in permanent metabolic abnormalities in fetal metabolic tissues and organ systems with a subsequent predisposition to cardiometabolic disease. This process is known as metabolic programming.

As previously discussed, conditions such as diabetes mellitus and obesity can lead to macrosomic fetuses or fetuses with increased birth weight owing, in part, to an increase in adipose tissue development. The hyperglycemic maternal environment stimulates the fetal pancreas to produce insulin, and the fetus subsequently develops hyperinsulinemia, prompting increased development and deposition of adipose tissue. Interestingly, some studies have shown that any increase in maternal glucose concentration, even in the

normal range, is associated linearly with increased fetal adiposity and birthweight [33]. There is also evidence to suggest that these increases in maternal glucose concentration within the normal range may also predispose the exposed fetus to develop diabetes mellitus, overweight, and obesity, independent of maternal BMI [34].

1.3.1 Cardiovascular Disease (CVD)

CVD is the number one cause of death worldwide and is composed of a group of disorders affecting the heart and blood vessels of the body. Coronary heart disease, cerebrovascular disease, peripheral arterial disease, and deep vein thrombosis are all examples of CVDs. Risk factors for developing CVD include consumption of a poor diet, physical inactivity, obesity, tobacco use and genetic factors. Two serious consequences of CVD are myocardial infarction (heart attack) and cerebrovascular accident (stroke) most often caused by a narrowing of the blood vessels supplying the heart or brain due to atherosclerosis. Atherosclerosis is the accumulation of fatty deposits within the blood vessel walls [35].

1.3.2 Type II Diabetes Mellitus (Type II DM)

Type II DM is a leading cause of death in North America, and the global prevalence of the disease is rapidly rising. It is characterized by abnormally high levels of glucose in the blood and reduced sensitivity of the body's cells to insulin, known as insulin resistance. Normally, when levels of glucose are increased in the blood, the pancreas is stimulated to release insulin. Circulating insulin controls glucose levels and drives glucose from the blood into cells for use as energy or storage once energy needs for the body are met. With type II DM, the body's cells are not as responsive to insulin, and excess glucose remains in the blood. As this resistance to insulin develops, beta cells in the pancreas produce more insulin to normalize blood glucose levels. Eventually, the pancreatic beta cells become less capable of responding to fluctuations in blood glucose levels, and there is a shortage of insulin. This insulin shortage prevents the effective reduction of glucose levels in the blood.

The aging process and genetic factors involving gene expression are associated with an increase in the risk of developing type II DM and will exacerbate the metabolic

dysregulation characteristic of the condition. Other factors such as poor diet, overweight and obesity, and physical inactivity also increase the risk and exacerbate the metabolic dysregulation. However, these factors also increase the risk of developing type II DM at any age. Uncontrolled type II DM can lead to severe health conditions such as CVD and eye, nerve, and renal damage [36].

1.3.2.1 Fatty Liver Disease

Fatty liver disease refers to the excessive accumulation of lipids within hepatocytes above 5% of the total liver volume. Non-alcoholic fatty liver disease (NAFLD) refers to the condition where this abnormal accumulation of lipid in the liver cells is not attributable to alcohol consumption. Instead, the likelihood of developing NAFLD increases with being overweight or obese, with fat accumulation centred around the waist. Developing NAFLD is also associated with having type II DM and consuming a diet high in saturated fat and refined sugars regardless of BMI. As the liver processes sugars and fats from dietary intake for use as energy for the body, excesses are stored as lipids in the hepatocytes. This process may lead to enlargement of the liver and, eventually, the hepatic inflammation and fibrosis characteristic of non-alcoholic steatohepatitis (NASH). NASH can ultimately lead to cirrhosis of the liver, chronic liver failure requiring transplant, and liver cancer [37].

1.4 Obesity

Obesity is described as a chronic and progressive disease where excessive fat accumulates in the body that may harm our health. According to a 2014 health survey, 5 million Canadians were living with obesity, and that number is expected to increase over the next two decades. The annual direct healthcare cost for obesity-related medical care is approximately 7 billion dollars, and this cost is expected to rise to 9 billion dollars by the year 2021 [38].

Obesity is commonly measured using the body mass index (BMI). It is measured by dividing an individual's weight in kilograms (kg) by their height in metres squared (m^2), giving a result expressed in kg/m^2 . This result is then compared to a weight classification BMI chart to determine an individual's weight classification. A BMI above $30 kg/m^2$ is

generally accepted to represent obesity in the Caucasian population - though this is only a measure of size and not health. Other factors, such as waist circumference, waist-to-hip ratio, and the presence of associated co-morbidities, should also be considered when making a formal medical diagnosis of obesity. A diagnosis of obesity is associated with the consumption of a Western diet and is also associated with co-morbidities such as type II diabetes mellitus, hypertension, cardiovascular disease, and infertility [38, 39].

As the rates of obesity in the general population increase, obesity rates in females of child-bearing age also continue to rise. Obese pregnancies are considered by the medical community to be “high risk” for serious maternal and fetal complications [40].

1.4.1 Obesity and Pregnancy

Obesity during pregnancy is the most common pre-existing health condition encountered by health professionals. The risk of developing conditions such as gestational diabetes mellitus and preeclampsia is increased in obese women when compared to normal-weight women. As such, fetal congenital anomalies, early spontaneous abortions, and IUGR and macrosomic fetuses are more likely to occur in obese women. Infertility is also more prevalent in obese women than in normal BMI women. This increased prevalence may be due to changes in the menstrual cycle, the quality of oocytes ovulated from the ovaries, and an unfavourable endometrial environment for implantation and development of the conceptus within the uterus [19].

Obesity in pregnancy is implicated in long-term effects on the fetus. Early pregnancy alterations to fetoplacental metabolic programming can increase the risk in the offspring of developing conditions such as type II diabetes mellitus, cardiovascular disease, and obesity throughout their lifespan. This increased risk seems to be the result of metabolic dysregulation in the maternal environment. Increased insulin resistance results in decreased uptake of glucose into the tissues for energy metabolism. Subsequent increases in lipolysis for energy metabolism contribute to a lipotoxic environment and represent a dysregulated metabolic state. It is thought that this metabolic dysregulation is a contributing factor to the epigenetic changes in fetoplacental metabolic programming

and may even be damaging to the placental tissues, affecting the development and function of the placenta [19].

1.5 Western Diet

The term “diet” refers to the types of food habitually consumed by an individual or by a whole community. The foods we consume provide us with energy and nutrients, such as glucose and vitamins and minerals that help our bodies to maintain homeostasis. Our bodies require energy and nutrients derived from the foods we consume, to maintain proper growth and functioning of our organ systems and also, in times of stress, illness, or damage to protect us from harmful agents and repair damaged cells.

The quality and composition of one’s diet are paramount to our health and a significant factor in whether or not we develop many largely preventable diseases, such as cardiovascular disease or type II diabetes mellitus. A nutritionally complete and metabolically healthy diet is composed mostly of a wide variety of fruits, vegetables, legumes, and complex carbohydrates with relatively small amounts of meat, seafood and fish, and dairy. This type of nutritionally rich diet provides us with the nutrients and metabolically healthy energy sources we require while being naturally low in saturated fats and simple carbohydrates, which are detrimental to our metabolic function [41, 42].

Over the last few decades, there has been an increasing trend towards highly processed, fast-food-type diets in many developed countries that are strongly associated with the current obesity epidemic in North America. These diets are commonly referred to as the Standard American diet and the Western diet. These diets are widely available and widely consumed intermittently and habitually.

Typically, a WD is high in fat content, high in refined sugars, and high in red meat content while being low in dietary fibre and having very few fruits, vegetables, and legumes. Overall, this is a nutritionally poor, calorically dense diet that is not compatible with our energy and nutritional requirements. Habitual consumption of a WD is strongly associated with obesity, cardiovascular disease, and type II DM [43, 44].

Again, just as consumption of a WD has the potential to impact the health of non-pregnant adults and children negatively, it will also likely impact the fetoplacental unit in a critical period of growth and development.

1.5.1 Western Diet for an Animal Model of Pregnancy

In this thesis, pregnant guinea pigs were used as an animal model for the human fetoplacental unit. Either a control diet (CD) or a Western diet was fed *ad libitum* to the pregnant guinea pigs for their lifetime. Both the control and Western diet feeds for the guinea pigs were pelleted and soy-based, with the WD being energy-dense. Percentages of dietary protein, carbohydrate, and fats (PUFAs- polyunsaturated fatty acids, MUFAs- monounsaturated fatty acids, and SFAs- saturated fatty acids) that compose the two diets are designed to mimic, as closely as possible, a cardiometabolically healthy diet as a control and a Western diet for a guinea pig model of pregnancy [45, 46]. Figure 5 illustrates the components of the control and Western diets.

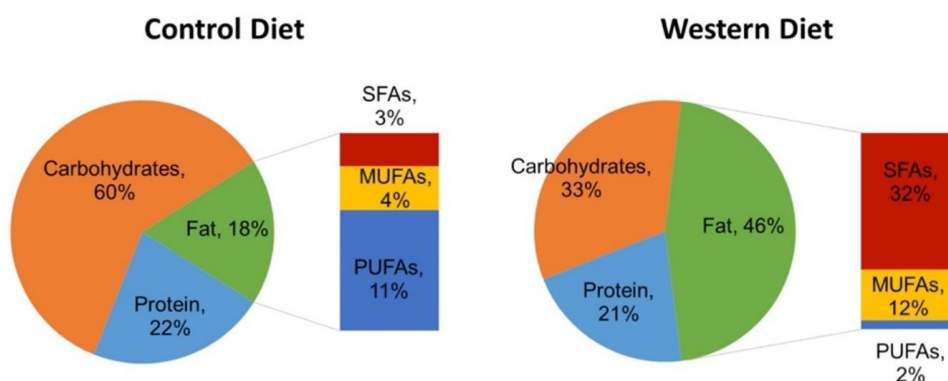


Figure 5: This figure demonstrates the percentage composition of carbohydrates, fats, and protein in the control and Western diets [7, 45].

1.6 Guinea Pig (GP) Model of Pregnancy

There are several possible models of pregnancy. Most notably, sheep and rodents have often been preferred as a model because of their similarities to the human gestational process and are, therefore, most apt to provide information that can be translated to the human gestational period [47]. However, these models have several disadvantages. Translational research concerning the developmental origins of health and disease

requires a small animal model with a relatively short life span compared to humans. Sheep take a longer time to reach maturity and present more significant challenges concerning housing and management compared to other small animal models. Rats and mice, while more suitable than sheep in terms of size, complete key stages of development post-natally in contrast to the prenatal development seen in humans. Additionally, mice and rats tend to have large litters of 8-12 pups- a characteristic considered undesirable for clinical translation of research. Guinea pigs (*Cavia porcellus*), another type of rodent, are small animals, have relatively smaller litter sizes of 1-5 pups, are prenatal developers and have also emerged as a suitable model of pregnancy given their many structural and functional similarities to humans, as well as similarities in their physiological response to insults [47].

While the gestational period of a guinea pig (GP) is ~69-71 days compared to the ~40-week gestation of a human fetus, its fetal developmental timeline and process is broadly similar to that seen in the human fetus. For example, the fetal GP accumulates both brown and white adipose tissue in utero and has a high total fat content at birth, unlike other rodents and sheep. Another critical similarity to humans is the placental structure and function. The GP placenta is haemomonochorial, meaning that there is a single layer of chorionic cells separating maternal and fetal circulation of red blood cells. This type of separation between maternal and fetal blood circulation is analogous to the haemochorial placenta seen in humans. Also similar to the human placenta, the GP placenta has deep decidual invasion and similar cell columns of the anchoring chorionic villi in the subplacenta, among other structural similarities. Other rodent models lack the deep decidual invasion by the placenta seen in guinea pig and human pregnancy [47]. Functionally, the placenta in GPs has similar metabolism to humans and supports the pregnancy through the provision of progesterone throughout the major part of pregnancy, similar to humans but unlike mice, rats, and sheep, who rely on progesterone produced from the ovaries to maintain pregnancy. Because exposures to insults, such as an adverse maternal environment, can occur at a similar developmental stage, in a similar *in utero* environment, and with similar physiological responses to insults, the pregnant GP is considered to be an excellent model of human pregnancy [47].

1.6.1 Western Diet Association

It has been established that the metabolic dysregulation seen with obesity during pregnancy can alter fetoplacental processes leading to unfavourable outcomes of pregnancy in the short and long term. The ongoing rise in rates of overweight and obesity in the developed world is strongly associated with the consumption of a Western diet, high in saturated fats and refined sugars and low in nutritional quality. It is acknowledged in the literature that while there are relatively fewer studies focussed on the effects of a nutritionally poor, calorie-dense diet on the fetoplacental unit, this type of diet likely exerts an independent effect on the fetoplacental unit regardless of other factors [26].

1.7 Current Monitoring Methods of Fetoplacental Health

Currently, clinical monitoring of the health of a pregnancy is centred around a patient interview and manual examination by a specialized health care provider. Referral for laboratory tests and ultrasound examinations are routine protocol or can be ordered as needed should a pathological condition be suspected [48]. The use of magnetic resonance imaging (MRI) in pregnancy is possible and can contribute valuable information, but clinical use of MRI in pregnancy is still uncommon. Imaging modalities such as x-ray are not recommended for use in pregnancy, except perhaps in extraordinary, emergency cases, owing to the increased risk of unfavourable outcomes from exposure to ionizing radiation in the fetus [49].

1.7.1 Diagnostic Medical Ultrasound

Diagnostic medical ultrasound is a widely used, non-invasive imaging modality that employs non-ionizing energy in the form of sound waves from 2-15 MHz in frequency to generate high quality, medically diagnostic images of the internal structures and organs of the human body. Diagnostic medical ultrasound is commonly used for the management of uncomplicated and complicated pregnancies alike. Some advantages of diagnostic medical ultrasound include its wide availability, relatively low cost, use of non-ionizing energy, relatively high spatial and temporal resolution, and its real-time imaging capabilities [50]. Through the use of ultrasound in pregnancy, health care

providers can interpret B-mode anatomical images to identify normal and pathological findings and make accurate quantitative measurements regarding the size and location of fetal and maternal structures. They can also accurately estimate gestational age and fetal weight and accurately estimate functional parameters such as blood flow velocity, vascular resistance, and vascular pulsatility and waveforms using Doppler ultrasound [1, 50].

Ultrasound also has some disadvantages. It is highly operator dependent; it clinically uses 2-D measurements for image interpretation rather than 3-D volume measurements, which more accurately reflect the ground truth [51, 52]; and it provides only limited *in vivo* functional information and no direct metabolic information.

1.7.2 Fetoplacental Diagnostic Medical Ultrasound Assessment

The fetoplacental unit is readily assessed using diagnostic medical ultrasound. As pregnancy is by nature a process of growth and development, the routine examination protocol and interpretation of image characteristics changes with gestational age. The echogenicity and tissue texture of the placenta are qualitatively assessed, and the fetal organs and structures are assessed for abnormalities. Some other common qualitative characteristics, such as the placental location in the uterus and fetal orientation, situs, and presentation, are also documented. Quantitative measurements include the crown-rump length (CRL), cervical length, distance from the placental edge to the internal os of the cervix, abdominal circumference (AC), fetal heart rate (FHR), biparietal diameter (BPD), femur length (FL), amniotic fluid index (AFI), and umbilical, *ductus venosus*, and middle cerebral artery (MCA) Doppler measurements. Late pregnancy assessment via ultrasound also includes the assessment of biophysical parameters, such as gross and fine fetal motor movements and attempted respiratory movements [1]. All of these assessments are made in an attempt to monitor and understand fetoplacental health, but much more information, including metabolic and tissue volume information, is required that is simply not available with current ultrasound technology and clinical protocols.

1.7.3 Magnetic Resonance Imaging

MRI is an imaging modality that typically relies on the signal generated from the displacement and return to thermal equilibrium of the nucleus of a hydrogen atom for its image contrast. However, imaging of nuclei other than hydrogen is possible. Signal generation is achieved by aligning the nuclei in the main magnetic field (B_0), with subsequent and repeated disruptions to their alignment by a radio-frequency (RF) pulse (B_1). The application of an RF pulse causes displacement of protons away from the z-direction and toward the x-y plane. The z-vector represents, by convention, the direction of the B_0 magnetic field. Following the RF pulse, the protons return to thermal equilibrium in a process known as relaxation.

Longitudinal relaxation refers to the regrowth of magnetization in the z-direction and its return to equilibrium. The length of time it takes to achieve equilibrium is equal to $5 \times T_1$. T_1 is an intrinsic characteristic of the substance or tissue being imaged. Transverse relaxation refers to the decay of magnetization away from the y- and x-directions. The length of time this takes is known as T_2 and T_2^* . Transverse relaxation time is affected by interactions with nearby protons, and T_2^* is also affected by inhomogeneities in the magnetic field. While T_2 is an intrinsic characteristic of the imaged substance, T_2^* is subject to extrinsic factors such as local field inhomogeneity. Generally, these tissue characteristics form the basis for the multitude of image contrasts that are possible with MRI [53].

1.7.3.1 Advantages/Disadvantages of MRI

MRI is a complex, diverse, and flexible imaging modality with many benefits and some disadvantages relative to other imaging modalities. Some disadvantages include high cost [54], lack of availability, lack of expertise - specifically in fetal imaging, long examination time, sensitivity to motion [55], and suitability for all patient populations in terms of patient body habitus and patient safety in a strong magnetic field. Some benefits include a multitude of available image contrasts with adjustable imaging parameters that allow the operator or physician to tailor the acquisition to their needs; unsurpassed tissue contrast; the capability for reliable 3-D volume acquisitions; its use of non-ionizing

energy; its ability to provide structural and functional information about our bodies, including metabolism; and its multinuclear capabilities [53, 56, 57].

While diagnostic medical ultrasound remains the most common imaging modality employed throughout pregnancy, the use of MRI- specifically hyperpolarized carbon-13 (^{13}C) MRI has the potential to provide complementary *in vivo* metabolic information that could serve as a biomarker for fetoplacental health.

1.7.3.2 Anatomical Imaging

As previously mentioned, MRI can generate many different image contrasts. Some of these include diffusion-weighted imaging (DWI), proton density (PD) weighting, T_2 -weighted (T_2 -w), and T_1 -weighted (T_1 -w). The weighting of an image contrast refers to the tissue characteristics that are allowed to, by manipulation of imaging parameters, dominate the resulting image signal intensity. For example, in a T_1 -w image, parameters such as repetition time (TR) and echo time (TE) can be adjusted to capitalize on the effects of T_1 while minimizing the effects of T_2 on image contrast. Typically, T_1 -w images provide high resolution, detailed anatomical information, including visualization of pathology. T_2 -w images provide the same type of information as T_1 -w images, but are generated mostly from T_2 tissue characteristics and are complementary to T_1 -w images [53].

1.7.3.3 Carbon-13 (^{13}C) and MRI

While conventional MRI utilizes the proton within the nucleus of a hydrogen atom to generate a signal, it is possible to generate a signal from the protons in the nucleus of other elements, such as carbon, which forms the backbone of many biological molecules. The natural abundance of carbon-12 (^{12}C) in tissues is 98.93%, similar to the abundance of hydrogen (^1H) at 99.98% [58]. However, ^{12}C is not visible on MRI due to its lack of nuclear spin, but its isotope, ^{13}C , is visible and has previously been exploited in research on cancer metabolism. MR imaging with ^{13}C has three main limitations. First, in the body, the atomic concentration of carbon is approximately $1/5^{\text{th}}$ of the atomic concentration of hydrogen. Therefore, the signal that can be obtained from carbon can be

no more than $1/5^{\text{th}}$ of the signal that can be obtained from hydrogen, since there are $1/5^{\text{th}}$ as many carbon nuclei as hydrogen nuclei present in the body to generate a signal. Second, the natural abundance of ^{13}C in the body is extremely low, at 1.11%. Since the MRI signal is proportional to the number of ^{13}C nuclei in an image voxel, the signal detected from ^{13}C is substantially lower than the signal that can be detected from ^1H . Finally, the signal obtained is proportional to the gyromagnetic ratio, which for ^{13}C , is roughly one-quarter of the gyromagnetic ratio of ^1H (Table 1). Again, this results in very low levels of signal from ^{13}C and makes *in vivo* MR imaging very challenging because the ^{13}C signal relative to ^1H is approximately equal to $1/5 \times 1/100 \times 1/4$ of the ^1H signal or 0.05% of the ^1H signal [59].

Table 1: Comparison between ^1H and ^{13}C natural abundance, gyromagnetic ratio, and relative signal strength.

NUCLEUS	^1H	^{13}C
Natural Abundance	99.98%	1.11%
Gyromagnetic Ratio (MHz/T)	42.58	10.71
Relative Signal Strength	1	0.0005

1.7.3.4 Hyperpolarized ^{13}C Imaging

Even though MR has limited sensitivity to endogenous ^{13}C , methods can still be employed to take advantage of the biological information that can be obtained from ^{13}C MRI. First, rather than depending on endogenous ^{13}C to generate signal, highly-enriched, ^{13}C -labelled molecules such as pyruvate can be introduced to the biological system. Typically, supra-physiological amounts of the labelled agent are required for distribution throughout the tissues of interest. Additionally, the enriched and labelled agent can be hyperpolarized. Hyperpolarization is the process of enhancing the magnetization of a sample. It is achieved by increasing the degree of alignment of the sample's nuclei within

the magnetic field beyond the degree of alignment possible at thermal equilibrium [59]. Though there are a few methods of hyperpolarization, dynamic nuclear polarization (DNP) is used in this thesis.

1.7.3.4.1 Dynamic Nuclear Polarization (DNP)

DNP is the transfer of spin polarization from highly polarized electrons to the surrounding nuclei. This polarization is achieved by irradiating the sample containing 100%-enriched ^{13}C molecules with microwaves at low temperatures (1.4K) and high magnetic field strength (3.35T). This process yields a frozen hyperpolarized sample. The frozen hyperpolarized solution must then be warmed rapidly to near body temperature by a process referred to as dissolution before *in vivo* administration. Recalling that the MRI signal generated from endogenous, unpolarized ^{13}C is approximately 0.05% of the signal that can be generated from ^1H , DNP increases the MRI signal of hyperpolarized ^{13}C solutions by 10,000-fold when compared to the signal possible at thermal equilibrium. Therefore, the process of hyperpolarization via DNP increases the signal to levels comparable to ^1H MRI, despite the small injected volume of the hyperpolarised sample, and makes ^{13}C MRI feasible [59].

1.7.3.4.2 [$1\text{-}^{13}\text{C}$] Pyruvate

While it is possible to label most biological molecules with ^{13}C for use as a hyperpolarized ^{13}C probe, some practical considerations need to be reviewed. First, the T_1 value of the hyperpolarized probe must be long enough to maintain magnetization for MRI before the signal decays away to thermal equilibrium. Second, as a probe of *in vivo* metabolism, the hyperpolarized solution must be rapidly administered to undergo metabolism in the tissue of interest before imaging begins. As such, the T_1 value of the ^{13}C nuclei itself is of critical importance. In ^{13}C -labelled pyruvate, the T_1 is on the order of tens of seconds. By the time $3xT_1$ has elapsed, 95% of the signal has already been lost. Therefore, the sample of hyperpolarized solution must be transported to the MRI unit, injected, distributed to tissues of interest via the vasculature, and metabolized quickly to take full advantage of the signal generated by a hyperpolarized ^{13}C probe. Lastly, the position of the ^{13}C -label on the carbon-based molecule has implications for the observed chemical shift of the molecule and alters the metabolic pathways that can be probed.

[1-¹³C] pyruvate (¹³C label on the C₁ carbon position of pyruvate) is the hyperpolarized ¹³C probe most commonly used for *in vivo* metabolic imaging as it addresses the challenges listed above. The C₁ of pyruvate has a T₁ of approximately 65s at 3T. This T₁ is relatively long and ensures sufficient magnetization of the ¹³C-labelled pyruvate is available for signal generation during administration and metabolism. Next, pyruvate is a crucial metabolite at the intersection of several critical metabolic pathways. In addition to these properties, pyruvate with a single ¹³C label has a single spectral peak for each of its metabolites that are well-separated by chemical shift. These separated single peaks allow for accurate quantification of metabolic conversions from pyruvate to its metabolites.

The use of [1-¹³C] pyruvate permits the probing of glycolysis as it pertains to the conversion of pyruvate to lactate, alanine, and acetyl-CoA via the PDH reaction with CO₂ as a by-product. It does not, however, allow for probing of the TCA cycle because the [1-¹³C] label does not transfer to the metabolites involved in the TCA cycle as the labelled pyruvate is metabolized. This lack of label transfer to metabolites makes the TCA cycle invisible when using a [1-¹³C] pyruvate solution [59]. To probe the TCA cycle, the C₂ of pyruvate must possess a ¹³C label [60].

1.7.3.4.3 Hyperpolarized MRI Sequence- BB IDEAL

There are many different types of MRI sequences designed to capture specific information. To gather metabolic information using a ¹³C hyperpolarized solution, a broadband iterative decomposition of water and fat with echo asymmetry and least-squares estimation (BB IDEAL) acquisition and reconstruction has proven to be effective. BB IDEAL is a chemical-shift-encoded sequence that is a variation on the IDEAL sequence, which ordinarily quantifies the fat and water content of tissues. For this adaptation, instead of separating the signal from fat and water, the BB IDEAL reconstruction separates the signal coming from pyruvate, lactate, alanine, and bicarbonate based on their known chemical shift using an expanded Dixon method. BB IDEAL MR is a gradient-echo sequence with a spiral-pattern, center-out collection of k-space data that provides 3-D proton density (PD) weighted images [61].

1.7.3.4.4 Area Under the Curve (AUC)

The AUC is a data analysis method that permits the quantification of rates of metabolism of hyperpolarised substrates. For this thesis, the AUC is the sum-over-time of the PD-weighted signal for each respective metabolite in a time-resolved data set. The ratio of the AUC for pyruvate to the AUC of each metabolite provides the lactate-, alanine-, and bicarbonate-to-pyruvate ratios - the LPR, APR, and BPR, respectively. These AUC ratios represent the relative signal intensity of each metabolite throughout the BB IDEAL MR acquisition. These normalized AUC ratios are directly proportional to the rate constants of conversion from pyruvate to lactate, alanine, and bicarbonate, given as the k_{PL} , k_{PA} , and k_{PB} , respectively [62]. This proportionality exists because the metabolic reactions under examination represent first-order reactions in terms of enzymatic activity. A first-order reaction means that the concentration of the catalyzing enzyme is proportional to the first power of substrate concentration [catalyzing enzyme] \propto [substrate¹]. Thus, the amount of enzymatic activity and resultant metabolite production (i.e., lactate, alanine, bicarbonate) is not limited by the amount of substrate (i.e., pyruvate) present [63].

1.8 Objective and Hypothesis

The objective of this thesis was to investigate the relationship between maternal Western diet consumption and placental metabolic function and to quantify metabolic function using hyperpolarized ¹³C MRI in a guinea pig model of pregnancy.

This thesis postulates that lifelong maternal consumption of a Western diet perturbs placental metabolic function, resulting in an increase in the conversion rate of pyruvate to lactate and alanine (k_{PL} and k_{PA} , respectively) and a decrease in the conversion rate of pyruvate to bicarbonate (k_{PB}).

Chapter 2

2 Assessing Mid-pregnancy Placental Metabolism and Physical Characteristics in Guinea Pigs Fed a Lifelong Western Diet

In this study, conventional MRI and hyperpolarized ^{13}C MRI were used to assess mid-pregnancy placental metabolism, appearance, and volume. Pregnant sows were fed either a control or Western diet to ascertain the effects of diet consumption on placental metabolism and physical characteristics.

2.1 Introduction

Throughout the gestational period, pregnancies can develop complications, which can negatively impact the fetoplacental unit. Some of these complications are related to *in utero* environmental exposures of the fetoplacental unit to external toxins or an unfavourable maternal environment. One factor that has the potential to affect the condition of the maternal environment, which ultimately impacts the fetal environment, is the consumption of a Western diet [64].

When challenged, cellular metabolic flexibility enables cells to adaptively utilize metabolic pathways to maintain energy status and physiological function [31]. Numerous disease states see metabolic flexibility as a hallmark of the physiological and pathological alterations affecting cellular function and survival through induction of a “glycolytic shift.” This shift means cells will favour the production of ATP by glycolysis instead of ATP production via oxidative phosphorylation [65]. Pyruvate is a central metabolite for cellular metabolism. It is produced in the cytoplasm, mainly by glycolysis, and exists in equilibrium with alanine and lactate [30].

Consumption of a WD, which is high in saturated fat and refined sugar, during pregnancy is associated with metabolic and mitochondrial dysregulation in maternal and fetal placental compartments at term [66]. This study sought to investigate if a glycolytic shift, early in pregnancy, might exist and possibly underlie late-pregnancy metabolic dysregulation. Hyperpolarized ^{13}C MRI techniques have been used to image metabolism

in pregnancy[67], but only normal pregnancies were investigated. Hyperpolarized ^{13}C MRI techniques have previously been successfully used to identify a glycolytic shift in human prostate cancer studies [68]. If a shift can be identified, technologies, such as hyperpolarized ^{13}C MRI, could provide a useful diagnostic tool in determining the severity of placental dysfunction and also help to understand the efficacy of treatments aimed at modulating the negative impacts of poor diet during pregnancy.

The development over gestation of placental metabolic processes, particularly pyruvate metabolism, are currently poorly understood. As such, this study aimed to quantify changes in the rate of conversion of pyruvate to lactate (k_{PL}), alanine (k_{PA}), and bicarbonate (k_{PB}) in a pregnant guinea pig (GP) model. It was postulated that lifelong consumption of a WD, in conjunction with pregnancy, would result in an increased mid-pregnancy placental k_{PL} and k_{PA} and a decreased placental k_{PB} . This hypothesis was derived from the idea that consumption of a WD and subsequent creation of a lipotoxic environment may lead to oxidative damage to the placental mitochondria. This damage may alter metabolic processes occurring in the mitochondria, such as the TCA cycle (part of aerobic cellular respiration). Damage to the mechanisms for aerobic cellular respiration may lead to increases in glycolytic activity (increases in lactate and alanine production) and decreases in aerobic cellular respiratory activity (decreases in bicarbonate) [14, 15]. Identifying alterations in placental metabolism may serve as a biomarker for fetoplacental metabolic health and provide us with knowledge regarding WD-exposed pregnancies not previously available.

2.2 Methods

2.2.1 Guinea Pig Model of Pregnancy

Data from 46 fetoplacental units from 15 pregnant sows, fed either a control or a Western diet lifelong, were collected. These sows were second-generation animals carrying their first viable pregnancies determined using diagnostic medical ultrasound. In this study, there were 33 fetoplacental units from 11 WD-fed sows and 13 fetoplacental units from 4 CD-fed sows.

2.2.2 Image Collection

Each sow underwent MRI at 33 days gestation (~mid term) with a term pregnancy being approximately 69 days. Animals were fasted 2 hours before MRI to ensure a similar metabolic state between sows. They were then given a 0.01mg/kg (body weight) dose of glycopyrrolate 30 minutes before MRI via subcutaneous injection to reduce saliva production by the sow and reduce the risk of aspiration when under anaesthetic.

Following the administration of glycopyrrolate, the GPs were anaesthetized using isoflurane. Anaesthesia was induced using a constant flow of 4.5% isoflurane and maintained with 1.5-2.5% isoflurane. The GPs were administered 2L/min of 100% O₂ for the duration of the experiment (~2.5 hours). An intravenous catheter was inserted into the saphenous vein of the left, hind foot to maintain vascular access for the injection of the hyperpolarized pyruvate solution.

The sows were secured in the prone position on a custom-built bed for MRI for the duration of the experiment and had their vital signs monitored using an animal monitoring kit (Small Animal Instruments, Inc.), containing a rectal thermometer, pulse oximeter, ECG leads, and respiratory pillow. The heart rate and electrocardiogram waveform, respiratory rate and respiratory waveform, percentage of oxygen saturation, the temperature in degrees Celsius were continuously observed and recorded periodically during the MRI scan. A single ECG lead, coated with electrode gel, was secured to the left and right front paws. The respiratory pillow was placed under the sows on their ventral aspect, near the location of the respiratory diaphragm, and a pulse oximeter was secured to the right hind foot. The lubricated thermometer was inserted rectally. The body temperature of the sows was maintained via a water-bath system containing two water pads with re-circulated heated water flowing through them. One pad was secured to the custom-built bed, underneath the sows, and the second pad was secured to the dorsal aspect of the sows. Foam earplugs were inserted into the right and left ear canals, and protective lubricant was applied to both eyes.

A series of MRI images were collected using a 3 T MRI (General Electric MR750), including T₁-w anatomical and BB IDEAL metabolic images. Following MRI, the sows

were allowed to recover and were humanely euthanized via CO₂ chamber ~48 hours post-MRI for the collection of fetal and maternal tissues for correlation.

The anatomical images were acquired with standard ¹H MRI, using a 32-coil cardiac array for data reception. The posterior half of the cardiac array was placed under the custom-built bed, and the anterior half of the cardiac array was placed over a plastic dome covering the sow and custom-built bed. A 3-D T₁-w spoiled gradient echo (SPGR) sequence was used to collect anatomical images with a scan time of ~8 minutes. These images served as an anatomical reference for manual segmentation of the placentae. This sequence had the following parameters as seen in Table 2: TR=5.1ms, TE=2.4ms, resolution=0.88mm, matrix=320 x 320mm, FOV=28 x 19.6cm. The field of view (FOV) was centred over the sow's abdominal region, ensuring visualization of all fetoplacental units.

Table 2: Summary of T₁-weighted imaging parameters.

IMAGING PARAMETERS	TR (ms)	TE (ms)	FOV (cm)	Matrix (mm)	Resolution (mm)
T ₁ -weighted Images	5.1	2.4	28 x 19.6	320 x 320	0.9 isotropic

2.2.2.1 Metabolic Images

Metabolic images were collected using a custom ¹³C birdcage coil (Morris Instruments). Before placing the sow in the ¹³C coil, the ¹³C coil was calibrated using the ¹³C acetate phantom signal and a free induction decay (FID) sequence to ensure visualization of the ¹³C signal. The ¹³C coil was then replaced with the ¹H array for anatomical imaging. Following anatomical imaging, the ¹H array was switched out for the ¹³C coil in preparation for the injection of the hyperpolarized [1-¹³C] pyruvate solution. The ¹³C coil was once again calibrated, this time using the signal from endogenous ¹³C in the sow to achieve the most accurate calibration. Loading the coil with the pregnant sow might have

altered the coil's calibration, so re-calibrating ensured the most accurate calibration for data collection. Following the preparation and administration of the hyperpolarized [^{13}C] pyruvate solution (see details in Section 2.2.3), metabolic images were acquired [61, 67].

A 3-D broadband IDEAL MRI sequence with a hybrid flip angle (HFA) scheme [69] was used to collect metabolic images for metabolite quantification and localization within the placenta. Over a 50 second scan time, seven metabolic images with 14 slices each were acquired at 7.5s intervals, using the acquisition parameters in Table 3. The FOV was centred over the sow's abdominal area to ensure the inclusion of all fetoplacental units. Table 4 contains the flip angle (FA) for each metabolite at each time point.

Table 3: Summary of the imaging parameters for the BB IDEAL images.

IMAGING PARAMETERS	TR (ms)	TE ₁ (ms)	Δ TE (ms)	ETL	FOV (cm)	Matrix (mm)	Slice Thickness (mm)	Resolution (mm)
BB IDEAL Images	16	4.5	1.1	4	20	24 x 24	8.5	8.3 in-plane

Table 4: Summary of hybrid flip angle scheme for metabolic image acquisition.

HYBRID FLIP ANGLE SCHEME	Time Point 1	Time Point 2	Time Point 3	Time Point 4	Time Point 5	Time Point 6	Time Point 7
	FA (deg)	FA (deg)	FA (deg)	FA (deg)	FA (deg)	FA (deg)	FA (deg)
Pyruvate	1.2	1.5	2	2.8	4.6	10	68
Lactate	1.2	1.6	2.1	3.2	5.4	13.4	88
Alanine	1.2	1.6	2.1	3.2	5.4	13.4	88
Bicarbonate	1.2	1.6	2.3	3.6	6.6	20.8	88

2.2.3 Hyperpolarized Injection

Following anatomical imaging, a 250mM hyperpolarized [1-¹³C] pyruvate solution, prepared via dynamic nuclear polarization using a Hypersense 3.35 T polarizer (Oxford Instruments), was dispensed into a flask. The weight-based dose (75mg/kg body weight), plus ~0.2mL, was drawn up in a 5mL syringe by M-E.E and transported to the MRI scanner (~30s) by L.M, L.S, or T.W. The pyruvate solution was then injected into the sow as a bolus through the previously inserted intravenous catheter over an ~12s period by L.F-W. The BB IDEAL imaging sequence was initiated manually using the key-pad at the bore of the magnet 7.5s after the injection began. Metabolic images were collected over the 50s scan time. The excess solution collected in the syringe was then flushed through the IV set with 0.9% saline, while an FID sequence (~1min scan time) was initiated to ensure *in vivo* hyperpolarization of the ¹³C signal.

The excess solution remaining in the flask after dispensation from the polarizer was drawn up in a separate 3mL syringe by M-E.E immediately following the collection of the weight-based dose, plus ~0.2mL. The excess solution was injected into the MQC

(Oxford Instruments) to ensure adequate polarization.

2.2.4 Analysis

Placental volume and characteristics, as well as litter size analyses, were completed using the T₁-w image acquisitions. The number of fetoplacental units visualized on MRI was determined using the T₁-w images and recorded on the experimental protocol form. BB IDEAL image acquisitions were used to analyze metabolic data. The pregnancy loss rate was determined using post-MRI collections data. However, in some instances, loss rate data was taken before fetal collections when the pregnancy was lost post-MRI but pre-collection. Pregnancy loss was confirmed either by ultrasound or visible discharge of the products of conception. The incidence of abnormal placentae was determined using the placental score (see Section 2.2.4.1.1). Nested statistical analyses were performed on the collected data using R (version 4.0.0) [70]. Only placentae having undergone successful HFA-metabolic MRI were included in the analyses.

2.2.4.1 T₁-w Analysis

M-E.E performed manual, full-volume segmentation of each placenta for placental localization using the collected T₁-w anatomical images and 3D Slicer (version 4.9.0) [71-74]. For each placenta, the volume, location relative to the maternal anatomy, and placental characteristics (see Section 2.2.4.1.1 below) were recorded.

2.2.4.1.1 Placental Characteristics and Scoring Analysis

The placental appearance was qualitatively evaluated and scored using the set of 6 binary criteria (score of zero or 1 for each criterion) in Table 5. These criteria were based on observable physical characteristics typical of normally-developed and healthy placentae in humans [1] and as observed in the majority of the CD-exposed placentae in the GPs. The following criteria were evaluated for each placenta. The overall visibility (Table 5: characteristic i) of each placenta was noted. A score of zero was given if the placenta was readily identified, and all aspects of the placenta were clearly visible and differentiated from surrounding tissues. A score of 1 was given if the placenta was poorly visualized and differentiated from surrounding tissue.

Next, placental border differentiation (Table 5: characteristic ii) was evaluated. The “border” refers to where the outer placental membrane meets the internal placental parenchyma. Placentae with well-differentiated placental borders were assigned a score of zero, and poorly differentiated placental borders were assigned a score of 1.

The third criterion evaluated the smoothness and regularity of the placental border (Table 5: characteristic iii). Smooth and regular borders were given a score of zero, and irregular or lobular borders were given a score of 1.

The next criterion evaluated the homogeneity of the placental parenchyma (Table 5: characteristic iv). Placental parenchyma observed to be homogenous was given a score of zero, and heterogeneous placental parenchyma was given a score of 1.

The fifth criterion evaluated the homogeneity of the MRI signal intensity between the placental parenchyma and border (Table 5: characteristic v). A score of zero was assigned if the observable difference in signal intensity between the placental parenchyma and border was non-existent or small. A score of 1 was assigned if the signal intensity of the placental border was perceived as being markedly hyperintense compared to the placental parenchyma.

The final criterion assessed was based on whether or not a complete fetoplacental unit (fetus and placenta) was readily discernable (Table 5: characteristic vi). Readily discernable fetoplacental units were given a score of zero. In cases where only a placenta could be visualized, a score of 1 was given. A score of zero indicated a “normal” appearing placenta or fetoplacental unit for that particular criterion. A score of 1 indicated a deviation from “normal” or an “abnormal” appearing placenta or fetoplacental unit for that specific criterion.

The maximum placental score was six, and the minimum placental score was zero. An overall placental score of zero indicated a normal-appearing fetoplacental unit. Any overall placental score of 1 or more indicated the presence of abnormal observable physical characteristics. Table 5 summarizes the scoring characteristics and the method of scoring.

Table 5: Summary of placental characteristics and scoring method.

PLACENTAL SCORING AND CHARACTERISTICS	i	ii	iii	iv	v	vi
Score=0	Readily visible	Differentiated	Regular	Homogeneous	Homogeneous	Yes
Score=1	Poor visibility	Poor differentiation	Irregular	Heterogeneous	Heterogeneous	No
Description	Overall visibility	Placental border differentiation	Placental border regularity	Placental parenchyma homogeneity	Homogeneity between placental parenchyma and border	Identification of complete fetoplacental unit

2.2.4.2 BB IDEAL Analysis

The metabolic images were reconstructed from the raw data set using the BB IDEAL reconstruction and MATLAB program (version R2019a) [75]. The placental volume segmentations generated from the T_1 -w images were then transferred to and overlaid on the reconstructed metabolic images to localize metabolite signals to the placentae. The AUC for pyruvate, alanine, lactate, and bicarbonate was calculated from the flip angle-adjusted mean metabolite signal intensities (SI_{FA}) in each placental volume at each of the seven time-points t using Microsoft Excel (2011) according to Equation 1:

Equation 1:

$$AUC_{metabolite} = \sum_t SI_{FA}(t)$$

Equation 2:

$$SI_{FA} = \frac{\text{Raw Mean Metabolite SI}}{\sin(FA)}$$

Though the AUC assumes a constant flip angle, Equation 2 corrects the signal to account for the metabolite-specific variable flip angles used with the HFA sequence. This adjustment means that the AUC ratio is still proportional to the rate constants of conversion for the metabolites.

The AUC ratios for each metabolite were calculated by dividing the AUC for each metabolite by the pyruvate AUC. The AUC ratio for each metabolite was assumed to be directly proportional to its respective rate constant of conversion from pyruvate to metabolite [62]. The AUC ratios for each metabolite were then compared between CD- and WD-exposed placentae using nested ANOVA analysis with Satterthwaite's method, with $\alpha=0.05$.

2.2.4.2.1 Litter Size, Pregnancy Loss/Success Rate, Incidence of Abnormality Analysis

The litter size for each sow was determined using T₁-w images from the time of MRI. Any discernible placenta, regardless of its physical characteristics, was included in the analysis. The mean litter size for both diet groups was then calculated by dividing the sum of the individual litter sizes by the total number of litters in the respective diet group. The litter size for each sow at collection was determined based on collections data and included only sows that maintained pregnancy until the time of euthanasia and collection. Pups deemed to be live, demised, or resorbing at collection were included in the litter size. The mean litter size was calculated using the same procedure as for the mean litter size at MRI.

The pregnancy loss rate was determined using a combination of post-MRI collections data and pre-collections data. The sum of fetoplacental units deemed to be demised or resorbing at the time of collection, in addition to pregnancies lost post-MRI but pre-collection (determined using litter size at MRI), was taken. This sum was then divided by the total number of placentae from each diet group and multiplied by 100. The pregnancy success rate was determined using collections data. Pups deemed to be "live" at the time of collection were included in this calculation. The sum of "live" pups at collection was divided by the total number of placentae from each diet group and

multiplied by 100. The incidence of abnormal placentae was calculated using the placental scores. Any placenta with a score higher than zero was considered abnormal. The sum of abnormal placentae was taken and divided by the total number of placentae in the respective diet group and multiplied by 100.

2.2.4.3 Statistical Analysis

Nested ANOVA and Welch's t-test statistical analyses of the data were generated using R (version 4.0.0)[70] for the placental score, diet, metabolic, volume and litter size data. The nesting method selected (Satterthwaite's method [76]) for the ANOVA accounted for the semi-dependent nature of the placentae within the same litter while avoiding inflating the *n* value artificially. Graphical representations of the data were generated using GraphPad Prism version 8.0.0 for Mac OS X, (GraphPad Software, San Diego, California, USA, www.graphpad.com) with $\alpha=0.05$. The litter size was analyzed using a simple mean calculation, as well as Welch's t-test. The loss rate and incidence of abnormality were analyzed using a simple percentage calculation.

2.3 Results

This section describes the results of the data analysis for the metabolic ratios, placental score, placental volume, litter size, pregnancy loss rate, and the incidence of placental abnormality.

2.3.1 Metabolite Production

APR and BPR (but not LPR) were found to vary significantly as a function of placental score. The APR and BPR increased significantly with increases in placental score. No significant variation was found in the LPR, APR, or BPR as a function of diet or placental volume. The p-values obtained from the nested ANOVA statistical analyses are summarised in Table 6. The LPR, APR, and BPR were calculated for every placenta included in the metabolic data. The WD group contained 33 placentae, and the CD group contained 13 placentae. The mean and standard deviation for the placental LPR, APR, and BPR are summarized in Table 7. The distribution of the data for the LPR, APR, and

BPR within the diet groups is represented in Figure 6. The distribution of the data for the LPR, APR, and BPR across placental score is represented in Figure 7.

Table 6: Summary of p-values for nested ANOVA statistical analyses. The titled columns represent contributing factors. The titled rows represent factors analyzed as dependent variables. * represents a statistically significant p-value

	Diet	Placental Score	Placental Volume
APR	0.19	0.031*	0.21
BPR	0.19	0.0061*	0.22
LPR	0.41	0.10	0.37
Placental Score	0.08		0.20
Placental Volume	0.26	0.076	

Table 7: Summary of the mean and standard deviation for the placental LPR, APR, and BPR.

Metabolic Ratio Mean+/-SD	LPR	APR	BPR
Western Diet	0.14+/-0.059	0.10+/-0.050	0.12+/-0.048
Control Diet	0.11+/-0.048	0.066+/-0.037	0.083+/-0.023

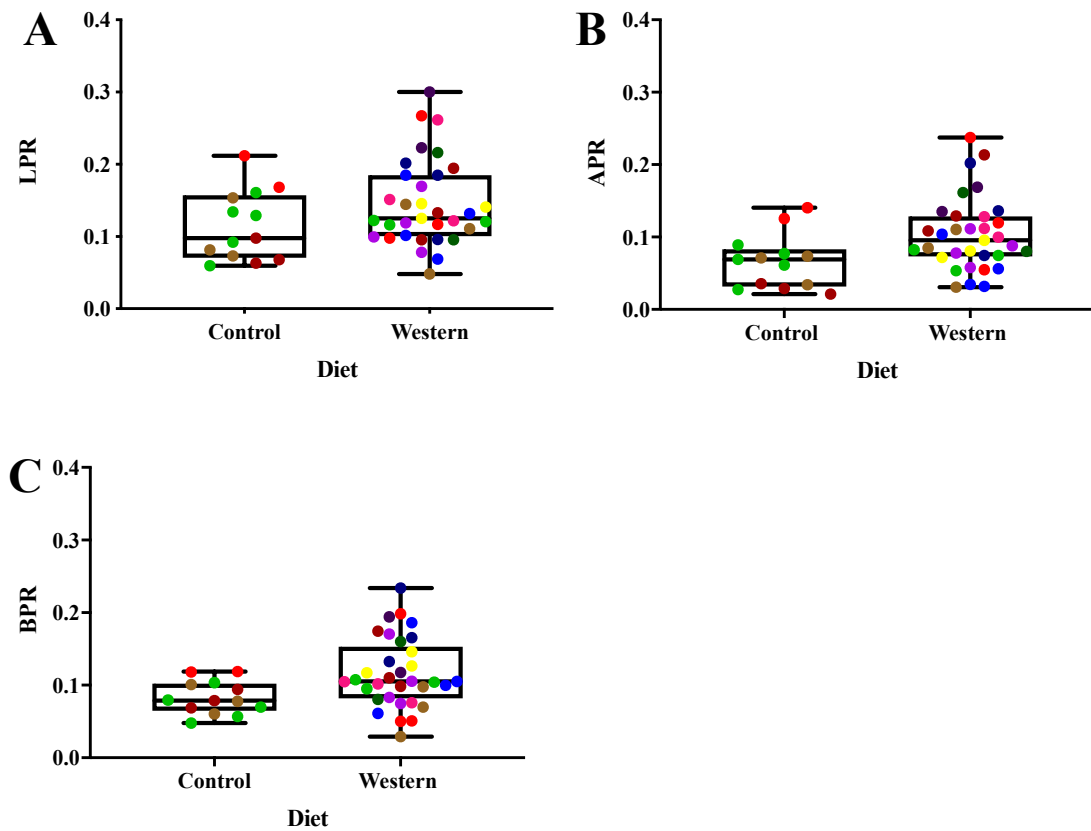


Figure 6: A-C. This figure demonstrates the distribution of the LPR (A), APR (B), and BPR (C) data in CD- and WD-exposed placentae. No statistically significant relationships were detected using a Nested ANOVA. Data points coded with the same colour within a diet group are part of the same litter.

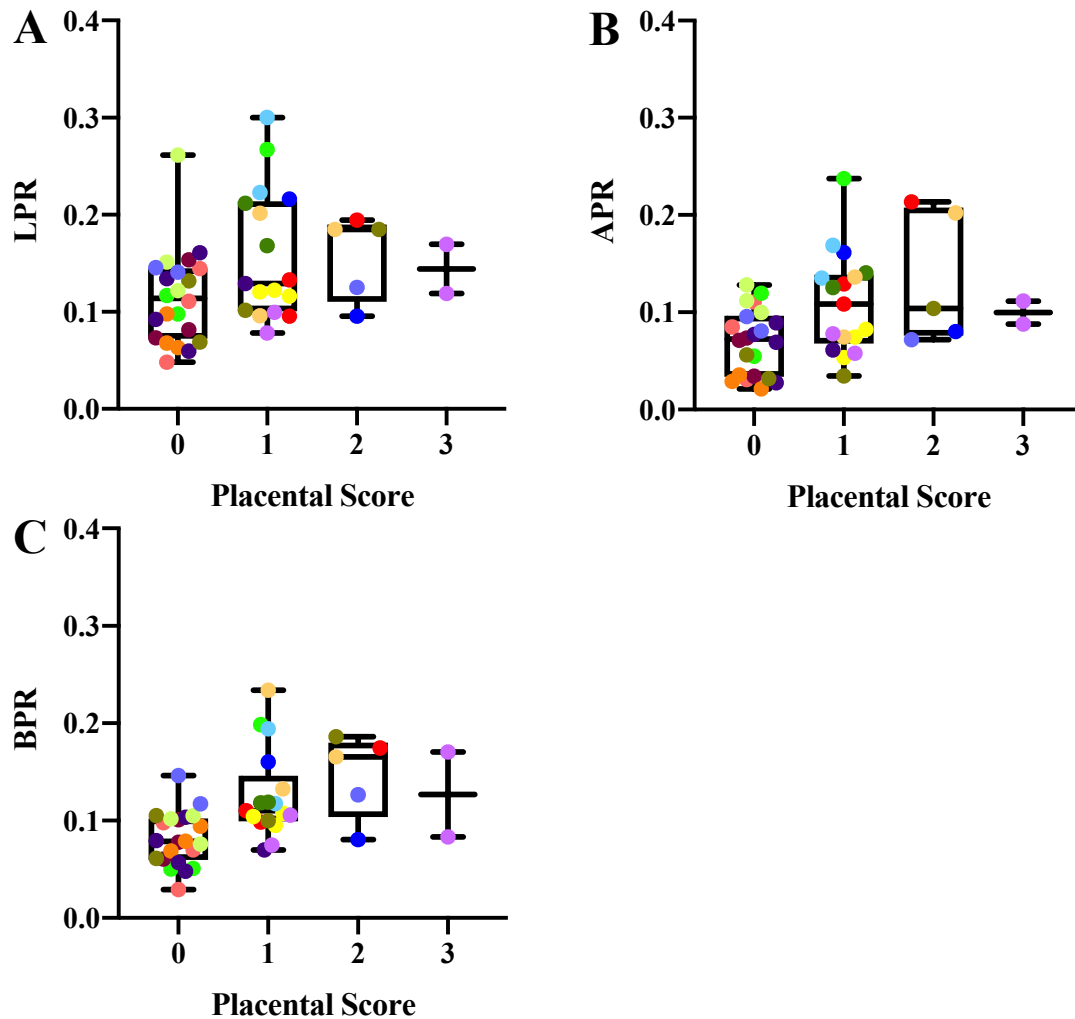


Figure 7: A-C. This figure represents the distribution of LPR (A), APR (B), and BPR (C) data across placental score. Data points coded with the same colour are part of the same litter. Statistically significant variation was detected for the APR (B) and BPR (C), but not for the LPR (A) using a Nested ANOVA.

2.3.2 Placental Score

The placental score did not vary significantly as a function of diet or placental volume. The mean placental score ($p=0.080$ for diet, $p=0.20$ for placental volume) in the WD group was 0.91 ± 0.88 (33 placentae total) and 0.23 ± 0.44 (13 placentae total) in the CD group. The distribution of the placental score data within the diet groups is represented in

Figure 8. Examples of normal and abnormal placental characteristics are demonstrated in Figure 9. Motion artefact is demonstrated in Figure 10.

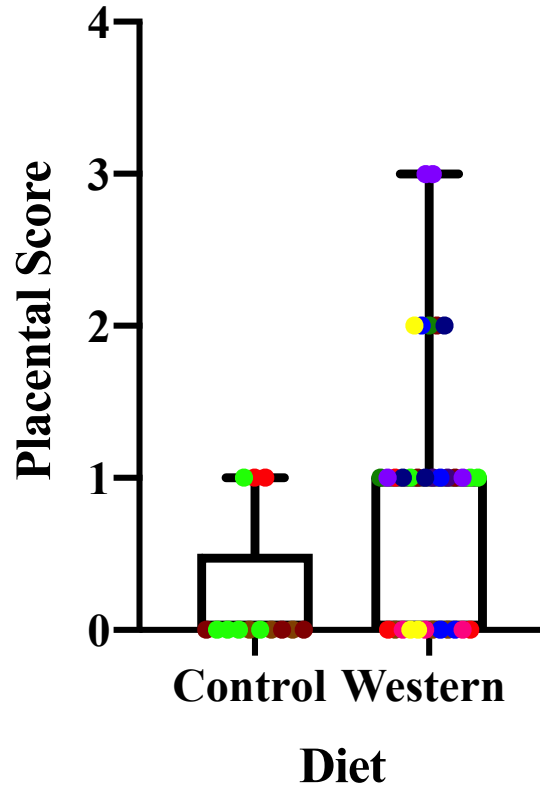


Figure 8: This figure demonstrates the distribution of the placental score data between CD- and WD-exposed placentae. No statistically significant relationships were detected using a Nested ANOVA. Data points coded with the same colour within a diet group are part of the same litter.

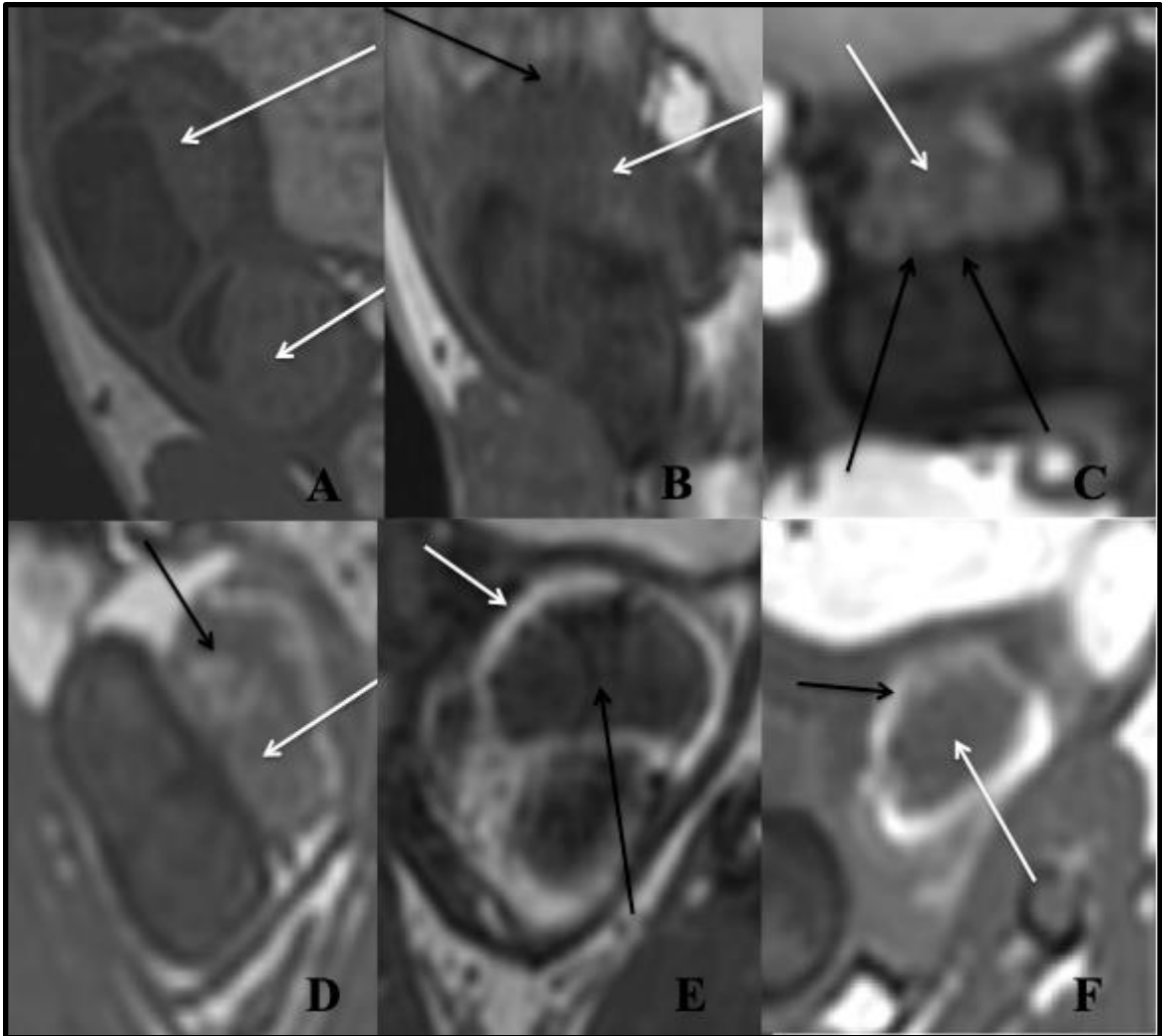


Figure 9: A-F. T₁-weighted images. A: demonstrates normal placentae. The white arrows indicate normal-appearing placentae. B: demonstrates characteristics i and ii from Table 5. The white arrow indicates a poorly visualized placenta. The black arrow indicates a poorly differentiated placental border. C: demonstrates characteristic iii from Table 5. The white arrow indicates the location of the placenta. The black arrows indicate an irregular placental border. D: demonstrates characteristic iv from Table 5. The white arrow indicates the location of the placenta. The black arrow indicates an area of heterogeneity with increased signal intensity relative to the rest of the placenta. E: demonstrates characteristic v from Table 5. The black arrow indicates the location of the placenta. The white area indicates a hyperintense placental border or "halo." F: demonstrates characteristic

vi from Table 5. The white arrow indicates the location of the placenta, and the black arrow indicates a hyperintense placental border. No discernible, associated fetus could be identified in this instance.

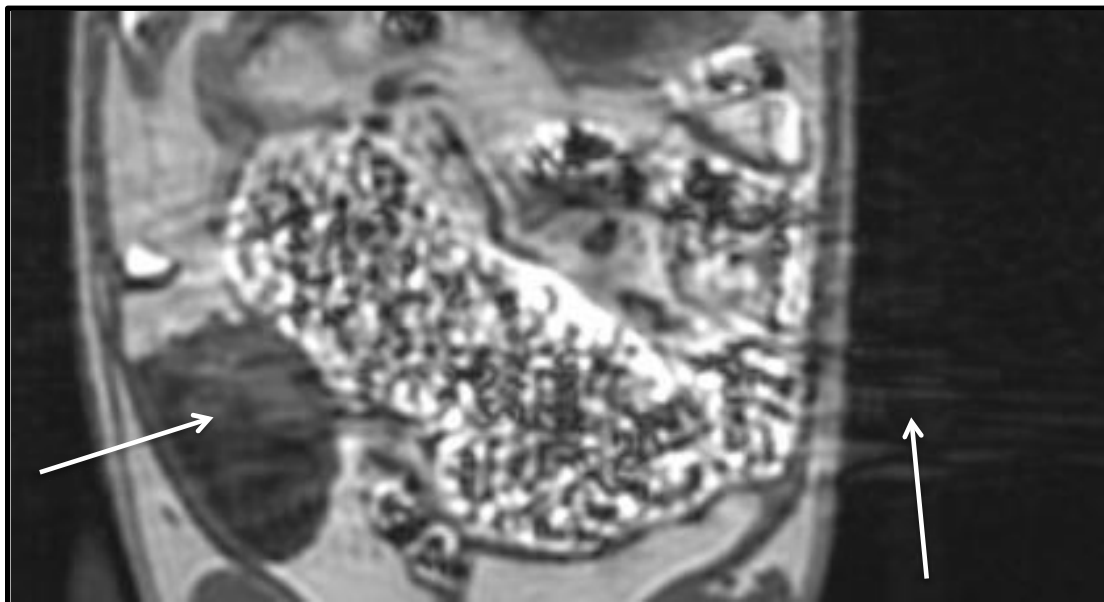


Figure 10: T₁-w image displaying motion artefact over the maternal abdominopelvic region. The white arrows indicate motion artefact both external to the sow and within the maternal abdominopelvic structures.

2.3.3 Placental Volume

The placental volume did not demonstrate significant variation as a function of diet or placental score. The mean placental volume ($p=0.26$ for diet, $p=0.076$ for placental score) in the WD group was $1.6\text{cc} \pm 0.82$ (33 placentae total) and $1.3\text{cc} \pm 0.22$ (13 placentae total) in the CD group. Placental volume data distribution within the diet groups is represented in Figure 11.

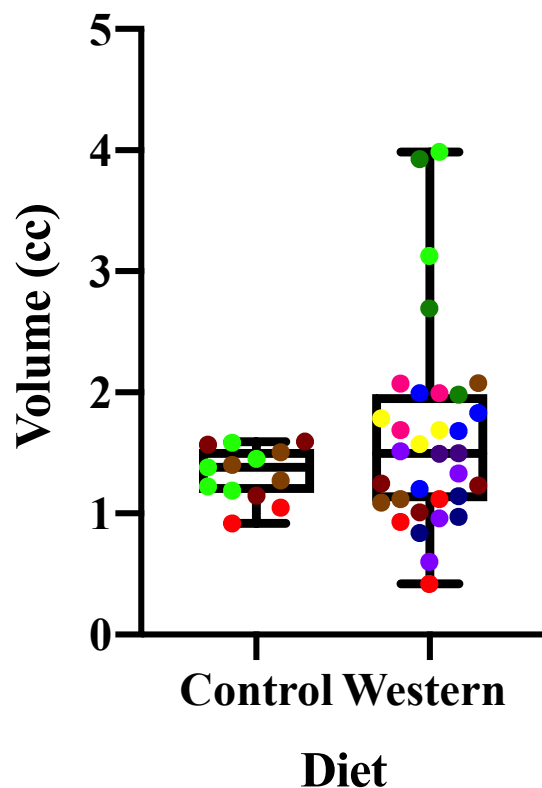


Figure 11: This figure demonstrates the distribution of the placental volume data between CD- and WD-exposed placentae. No statistically significant relationships were detected using a Nested ANOVA. Data points coded with the same colour within a diet group are part of the same litter.

2.3.4 Litter Size

A Welch's t-test in R (version 4.0.0) was used to analyze the litter size data. The litter size data at MRI and collection is represented in Table 8 and Table 9, respectively. No statistically significant differences in litter size at MRI or collection were detected between diets ($p=0.83$ at MRI, $p=0.97$ at collection). No statistically significant difference was found between the litter size at MRI and the litter size at collection in the WD group ($p=0.34$). There was no difference between litter size at MRI and litter size at collection in the CD group.

Table 8: Summary of the mean litter size data at the time of MRI.

MRI	Mean Litter Size (pups/litter)	Standard Deviation	Total Litters
Western Diet (11 litters)	3.1	+/-0.88	11
Control Diet (4 litters)	3.3	+/-1.3	4

Table 9: Summary of mean litter size data at the time of tissue collection.

COLLECTION	Mean Litter Size (pups/litter)	Standard Deviation	Total Litters
Western Diet (6 litters)	3.5	+/-0.84	6
Control Diet (4 litters)	3.3	+/-1.3	4

2.3.5 Pregnancy Loss Rate

In the WD group (31 placentae total), 74% of pups were demised or resorbed at the time of, or before collection, leaving 26% deemed to be live. The loss rate in the WD group is 2.4-fold higher than in the CD group. In the CD group (13 placentae total), 31% of pups were demised or resorbing before or at the time of collection, leaving 69% deemed to be live. The loss rate data is represented in Table 10.

Table 10: Summary of loss rate data.

LOSS RATE	Demised/Resorbed Fetoplacental Units	Live Fetoplacental Units	Total Placentae
Western Diet	74%	26%	31
Control Diet	31%	69%	13

2.3.6 Incidence of Abnormality

77% of CD-exposed placentae (13 placentae total) were deemed to be “normal,” and 23% were considered “abnormal.” In the WD group (33 placentae total), 36% of the placentae were considered “normal,” and 64% of the placentae were deemed to be “abnormal.” A 64% incidence of abnormality represents a 2.8-fold increase in the incidence of abnormality when compared to the CD group. The incidence of abnormality data is represented in Table 11.

Table 11: Summary of the incidence of placental abnormality data.

INCIDENCE OF ABNORMALITY	Normal Placentae	Abnormal Placentae	Total Placentae
Western Diet	36%	64%	33
Control Diet	77%	23%	13

2.4 Discussion

2.4.1 Metabolite Production

No statistically significant variations in metabolism were detected between the CD- and WD-fed groups. The inability to detect such variations was potentially because data from only one gestational age was examined. Data from later gestational ages may demonstrate more pronounced variations as fetoplacental needs vary across gestation. The use of data from a single gestational age was a limiting factor in this study, and data from later gestational ages should be analyzed in the future. Secondly, the small sample size, particularly in the CD group, likely impacted the statistical results of the study leading to a type II error. When this study was conceived, it was not clear that nested statistical analyses were necessary. Studies requiring nested statistical analyses typically require larger sample sizes. As such, the results of this study were not sufficiently powered to detect statistically significant variations.

Overall, metabolic, placental score, and volume data from WD-exposed placentae demonstrated large variability when compared to CD-exposed placentae. Despite the sows having been fed a lifelong WD, this variability may suggest that any potential effects and/or the severity of effects from WD consumption are variable between sows and between placentae from the same litter. The in-litter variability of the data implies that individual fetoplacental units may respond and adapt differently in a challenging *in utero* metabolic environment. The difference in response and adaptability between fetoplacental units from the same litter may be due to the semi-independent nature of fetoplacental units and genetic variation in a multiple-gestation environment. Fetoplacental units from the same litter may experience differences in their *in utero* environment. Most relevant to this study, variations in placental function, mainly diffusion, osmosis, and endocrine function, are reported in human studies on multiple gestation pregnancies where each fetus has a separate placenta [77]. Another possible source of in-litter variation may be related to sex differences between the pups. Animal studies using other rodent models have shown that male pups are more susceptible to challenging *in utero* environments, including maternal diet-related factors, such as high

fat and sugar diets. It is speculated that this increased susceptibility is due to variations in placental structure and function of male pups [78].

2.4.2 Placental Characteristics and Score

The placenta is a temporary organ that ages over gestation and functionally declines by the end of the gestational period. However, the placenta can age and decline in function prematurely due to exposure to some pathological processes and environmental factors, including preeclampsia, tobacco smoking, and diabetes [1]. Premature placental aging and decline can lead to deleterious outcomes of pregnancy and might alter placental function, including metabolism. The abnormal physical characteristics observed in the placentae are potentially the result of premature placental aging and decline. The T₁-w MR characteristics of the placentae were suggestive of placental aging [1]. Some characteristics of placental aging were consistent with a pathologist's findings in 40-day and 64-day GA WD-exposed placentae from a separate but similar study from a collaborator's laboratory. The pathologist (P.K) suggested that the histological findings might be suggestive of premature placental aging. Given the 2.8-fold increase in the incidence of abnormality in the WD-exposed placentae, the accelerated aging process of the placentae may be due, at least in part, to oxidative stress and formation of reactive oxygen species (ROS) induced by consumption of a WD (high fat and sugar). This metabolically toxic environment may damage the placental mitochondria and lead to mitochondrial dysfunction. Faced with chronic oxidative stress and ROS, placental tissue may enter cellular senescence. Cellular senescence is a process that prevents further cellular proliferation and regeneration and is a hallmark of cellular aging [79, 80].

The results presented in this study demonstrated statistically significant increases in the APR and BPR when a placenta was identified as having abnormal characteristics. In general, the trend revealed that as placental score increases, so does the APR and BPR. The increase in APR in abnormal placentae provides evidence to suggest an increase in placental ALT activity in those placentae [81]. When pyruvate and glutamate combine to form α -ketoglutarate and alanine as a by-product, ALT is used as the catalyzing enzyme [82]. The significance of the increased placental APR in the context of abnormal

placental characteristics remains unclear. However, increases in placental APR may be useful as a biomarker of fetoplacental metabolic health.

Though pyruvate is involved in energy production, in some instances of oxidative stress with ROS production, it functions as an antioxidant to neutralize ROS. As an antioxidant, pyruvate interacts with hydrogen peroxide to neutralize the ROS producing CO₂ and water as by-products. Though cells attempt to neutralize ROS using pyruvate, this process is often ineffective as the stimulus for oxidative stress, and ROS formation persists and overwhelms the cells [79]. The production of CO₂ (in equilibrium with bicarbonate) from the attempted ROS neutralization is potentially the source of the increased BPR. As such, increases in placental BPR may also be useful as a biomarker for fetoplacental health.

Placental scores were assigned to each placenta to indicate the presence or absence of observable physical characteristics deemed to be abnormal. A diverse range of characteristics considered abnormal was observed in the placentae of both CD- and WD-exposed placentae. While both diet groups contained placentae identified as being abnormal, a higher percentage (64%) of WD-exposed placentae were identified as being abnormal compared to (23%) of CD-exposed placentae. It should also be noted that WD-exposed placentae tended to possess more abnormal characteristics when compared to the CD-exposed placentae, leading to higher placental scores (>1) in the WD group. Several WD-exposed placentae were given placental scores of 2 or 3. The maximum score given in the CD group was 1. From this data, it seemed that maternal consumption of a WD had some association with the physical characteristics of the placentae though the nature of that association remains unclear.

Overall poor visibility and differentiation of the placenta from surrounding tissues, as well as poor differentiation between the placental border (plates) and parenchyma, may be the result of poor or declining placental function. Tissue differentiation in imaging studies is sometimes decreased or lost in the presence of chronic, progressive, or inflammatory disease. For example, chronic renal disease with functional loss can lead to poor corticomedullary differentiation on MRI as a result of a change in the tissue's T₁

value in a disease state [83]. Another possible cause for reduced visibility and differentiation and another limitation of this study was the motion artefact from the peristalsis of maternal bowel overlying the fetoplacental units. Active bowel has the potential to obscure or limit visualization of underlying and surrounding tissues. However, the rater (M-E.E) was careful to identify the presence of motion artefact and account for it when assessing the physical characteristics of the placentae.

An irregular, lobulated placental border is characteristic of an aging, declining placenta in humans. While placental aging and decline is a normal process, environmental insults, such as diabetes, can prematurely accelerate the process. Another characteristic common to the placental aging process and other pathological processes, such as hypertension and diabetes, is the development of placental infarcts. Infarcts are areas of tissue that have lost their blood supply. These infarcted areas may calcify or become necrotic [1]. On MRI, infarcts may appear as localized areas of hyperintensity. The presence of infarcted placental parenchyma may explain the observation of heterogeneous placental parenchyma.

The observed difference in signal intensity between the placental parenchyma and placental border, where the placental border formed a hyperintense “halo” surrounding the parenchyma, was potentially the result of a calcified placental border. Again, calcification of the basal and chorionic plates (placental borders) in human beings is part of the placental aging process but is concerning when it occurs before the later stages of gestation. Early calcification in the placentae is more likely the result of a pathological process rather than the normal, expected placental decline [1]. An alternate explanation for the hyperintense “halo” observed in some placentae is proteinaceous edema of the placental borders, perhaps due to an inflammatory process. Pathology reports from a collaborator’s laboratory indicated the presence of edema in the chorionic plate of a 64-day GA WD-exposed placenta. Though the pathologist (P.K) indicated that inflammation was not apparent, there was evidence of cellular debris from macrophages, which might suggest an inflammatory process.

In one case, a complete fetoplacental unit could not be confidently identified. However, the placenta was identified and segmented for volume, metabolic, and placental score data. This placenta appeared grossly abnormal. It is possible that the associated fetus was demised and had already been resorbed by the sow [84], making the identification of a complete fetoplacental unit impossible. However, it is also possible that the complex appearance of a grossly abnormal placenta in combination with often distended, gassy, complex, active maternal bowel obscured any potentially viable fetal tissues beyond recognition.

2.4.3 Placental Volume

As can be seen in Figure 11, there was considerable variation in the WD placental volume data when compared to the CD data. This variability may be attributable to variation in the effects of a WD on individual placentae within and between litters.

2.4.4 Litter Size

The total number of litters in the WD group varied between the mean litter size at MRI and the mean litter size at collection calculation because some sows had demonstrably lost their pregnancies before collection. The mean litter size at collection for the WD group was increased compared to the mean litter size at MRI because some fetoplacental units that were identified at the time of collection were not visualized on MRI. The inability to visualize some fetoplacental units on MRI may have been due to the complex appearance of the fetoplacental unit itself. It is also possible that the presence of complex, gassy maternal bowel obscured or limited the identification of a fetoplacental unit. Overall, the mean litter size between CD- and WD-fed sows was approximately equal, suggesting that diet did not affect litter size at 33-days gestation.

2.4.5 Pregnancy Loss Rate

For the loss rate calculation, 31 placentae were included instead of 33 placentae as in the metabolic data. Of the 33 placentae, one sow with three placentae was excluded from the loss rate calculation because the sow was found deceased post-MRI, and therefore the placentae were not included in the loss rate. One other placenta was added to the loss

rate calculation because it was not visualized on MRI but was identified upon collection. The 2.4-fold increase in fetoplacental loss in the WD-fed sows when compared to the CD-fed sows suggested that WD consumption might have been a factor in the successful maintenance of pregnancy. It could be speculated that the increase in loss rate was associated with the 2.8-fold increase in the incidence of placental abnormality in the WD-fed sows.

2.4.6 Incidence of Abnormality

The increased incidence of placental abnormality in the WD-fed sows suggested that WD consumption has some relationship with the physical characteristics observed on MRI and may contribute to premature placental aging. Consumption of a WD may also have more variable effects in a biological system that are dependent on other factors present in that system, accounting for the in-litter variability.

2.5 Conclusions

Lifelong consumption of a WD in pregnant GPs did not significantly affect placental metabolism, score, or volume. However, a significant relationship between the placental score and the APR and BPR was revealed. This relationship suggests that observing an increase in placental APR and BPR may be useful as a biomarker of fetoplacental health. The increased pregnancy loss rate in the WD-fed sows suggests that consumption of a WD is somehow associated with increased rates of pregnancy loss. The increased incidence of abnormality in the placentae of WD-fed sows suggests that WD consumption may contribute to premature placental aging and have more insidious placental effects than previously postulated. From this study, it is clear that additional data is needed to elucidate the relationship between lifelong WD consumption and fetoplacental health.

Chapter 3

3 Future Work and Summary

This section details future work that would help to clarify the relationship between lifelong WD consumption and fetoplacental health, such as the assessment of later gestational ages, the TCA cycle, and analysis of other fetal organs and tissues that may provide valuable information. A summary of the contents of this thesis is also provided.

3.1 Future Work

In Chapter 2, the glycolytic cycle was probed to quantify, indirectly, the conversion of [1-¹³C] pyruvate to lactate, alanine, and bicarbonate. The [1-¹³C] label was useful for this purpose. However, it was a limiting factor in that it was unable to provide critical metabolic information regarding the TCA cycle (a part of aerobic cellular respiration) because, chemically, the [1-¹³C] label does not transfer, through metabolic processes to the intermediate metabolites involved in the TCA cycle. In order to probe the TCA cycle, a [2-¹³C] label for pyruvate would be required. The [2-¹³C] label on pyruvate does metabolize to [5-¹³C] glutamate. In a reversible transamination process, glutamate converts to α -ketoglutarate- an intermediate metabolite of the TCA cycle. In this way, information about the integrity of the TCA cycle in a challenged metabolic state could potentially be investigated. Future studies employing a hyperpolarized [2-¹³C] pyruvate probe have the potential to broaden our understanding of placental metabolism, particularly as an indicator of aerobic cellular respiratory processes [60].

As detailed in Chapter 2, the metabolic activity, volume, and appearance of the placenta were examined. While this study provided valuable information regarding the metabolic health of the placenta and some of its physical characteristics, it did not examine relevant information from some other key metabolically-active organs and tissues. Namely, the maternal and fetal livers and adipose tissue were not examined in this study.

Consumption of a WD likely perturbs metabolism in such a way that metabolic pathways might be altered, stimulating ectopic lipid deposition in the fetal and maternal livers rather than in subcutaneous fat depots. Further studies could potentially examine the

integrity of the metabolic pathways within the maternal and fetal livers by quantifying the conversion of [1-¹³C]- and [2-¹³C] pyruvate to its spectrally visible metabolites. While this quantification is possible in the maternal liver, the presence of a metabolic signal in the fetal liver must be confirmed in order for this type of study to be feasible. The percentage of fat (or lipid) contained within the fetal and maternal subcutaneous, intra-abdominal, and intra-organ depots, and the volume of these tissues, should also be quantified. The volume of adipose tissue depots and liver volume can be obtained through manual segmentation. The percentage of fat or lipid in these tissues can be determined by quantifying the fat fraction derived from IDEAL (fat and water) MRI images. Qualitatively, tissue and organ appearance should be documented. The collection of this data would provide a more global assessment of maternal and fetal metabolic health, as well as provide morphological information regarding these tissues and organs.

Next, in this study, only one gestational age was considered (33-day, mid-gestation). Future studies should investigate [1-¹³C]- and [2-¹³C] pyruvate metabolism in the placenta and maternal and fetal livers (if possible); the volume and appearance of the placenta; subcutaneous, intra-abdominal, and intra-organ fat depots; and the fat fraction of these fat depots should be documented across gestation. Specifically, this information should be collected for 44-day and 60-day gestational age groups. This information may be useful in determining the progression of metabolic effects related to the consumption of a WD, as well as for comparison of metabolic effects between gestational age groups.

Finally, a major limiting factor of this study was the small sample size, considering the need to perform nested statistical analyses and the larger *n* required for such analyses to be accurate. In the future, additional data should be collected and analyzed in order to make confident conclusions about the relationship between diet and placental metabolism and characteristics.

3.2 Summary

This thesis investigated the effects of lifelong Western diet consumption during pregnancy on the placenta in a guinea pig model of pregnancy. The guinea pig is

considered an excellent model of human pregnancy because of its broadly similar fetal development and placental structure and function. The placenta is a critical and temporary fetal organ that acts as the maternal-fetal interface to support fetal growth and development. The placenta performs immunologic and endocrine functions, as well as providing nutrients to the fetus and allowing for gas exchange and waste removal.

Consumption of a WD, which is high in saturated fats and refined sugars and also nutritionally poor, is linked to alterations in fetoplacental metabolic programming, which may alter fetoplacental metabolism as an adaptive mechanism for short- and long-term survival. These metabolic alterations are linked to an increase in the lifetime risk that an exposed fetus will develop conditions such as CVD, obesity, and type II DM. It is postulated that consumption of a WD may lead to a lipotoxic *in utero* environment that results in the formation of reactive oxygen species and ultimately, oxidative damage to the placental mitochondria. This damage may necessitate the cellular use of alternate, less efficient metabolic pathways to meet fetoplacental energy requirements. As such, glycolytic pathways may be favoured over oxidative metabolism in a challenged *in utero* environment. An increase in glycolytic metabolism would result in increased lactate and alanine production and decreased production of markers for oxidative metabolism, such as bicarbonate.

Determining the potential metabolic effects of WD consumption is critical to understanding and preserving fetoplacental health. This relationship is currently poorly understood, but MRI imaging techniques, such as hyperpolarized ^{13}C MRI, may be able to provide valuable insight into fetoplacental metabolic health. Hyperpolarized ^{13}C -labelled pyruvate is a metabolic probe capable of evaluating the metabolic conversion of pyruvate to lactate, alanine, and bicarbonate. AUC ratios to quantify metabolite production can be derived from the MR images collected using the hyperpolarized ^{13}C -labelled pyruvate probe. These AUC ratios (LPR, APR, and BPR) are directly proportional to the metabolic rate constants of conversion from pyruvate to lactate (k_{PL}), alanine (k_{PA}), and bicarbonate (k_{PB}). In conjunction with anatomical T_1 -w MRI for placental localization and characterization, hyperpolarized ^{13}C MRI can indicate fetoplacental health status.

In Chapter 2, 33-day gestation (~mid term) pregnant sows underwent conventional proton and ^{13}C metabolic MRI to investigate the relationship between lifelong WD consumption and placental metabolism. Full-volume segmentations of the placentae were performed, and the placentae were characterized using anatomical T_1 -w MR images. Metabolite AUC ratios, proportional to their respective rate constants of conversion, were quantified from the metabolic hyperpolarized ^{13}C -labelled pyruvate images. A placental score, based on placental characterization, was assigned to each placenta. Mean litter sizes at MRI and tissue collection, as well as fetoplacental loss rate and the incidence of placental abnormality, were calculated. A statistically significant relationship was detected between the placental score and the APR and BPR but not the LPR. The APR and BPR may be useful as biomarkers of fetoplacental health. No statistically significant relationships were detected between the diet consumed and metabolite production, placental score, volume or litter size at MRI and collection. Considerable variability was noted in the WD group data between sows and within litters. Mean litter size was similar between diet groups; however, pregnancy loss rate and incidence of placental abnormality were increased in WD-exposed pregnancies. This study was limited by small sample size. An additional limitation was the use of data from only one gestational age. Future work should focus on increasing the sample size, including 44-day and 60-day gestational ages in the data analysis, including other maternal and fetal organs in the data analysis, and broadening the investigative scope of the metabolic probes.

Understanding and preserving fetoplacental health is critical for our short- and long-term health, as well as for future generations. It is clear that continued, focused research is necessary to clearly define the relationship between diet and metabolism throughout pregnancy.

References

1. Stephenson, S.R., *Diagnostic Medical Sonography, Obstetrics and Gynecology*. Third Edition ed. 2012, Baltimore, MD: Lippincott Williams & Wilkins.
2. ACOG. *How Your Fetus Grows During Pregnancy*. 2020. [cited April 2020]; Available from: <https://www.acog.org/patient-resources/faqs/pregnancy/how-your-fetus-grows-during-pregnancy>.
3. Symonds, M.E., et al., *Adipose tissue and fetal programming*. *Diabetologia*, 2012. **55**(6): p. 1597-606.
4. Herrick, E.J. and B. Bordon, *Embryology, Placenta*, in *StatPearls*. 2020: Treasure Island (FL).
5. Soares, M.J., K.M. Varberg, and K. Iqbal, *Hemochorial placentation: development, function, and adaptations*. *Biol Reprod*, 2018. **99**(1): p. 196-211.
6. DataBase Center for Lifescience. *Placenta*. 2014.
7. Creative Commons. *Attribution 4.0 International*. 2020; Available from: <https://creativecommons.org/licenses/by/4.0/>.
8. OpenStax College. *Illustration from Anatomy and Physiology*. 2013. [cited 2020]; Available from: <http://cnx.org/content/col11496/1.6/>.
9. Creative Commons. *Attribution 3.0 Unported*. 2020. [cited 2020]; Available from: <https://creativecommons.org/licenses/by/3.0/>.
10. Gathiram, P. and J. Moodley, *Pre-eclampsia: its pathogenesis and pathophysiology*. *Cardiovasc J Afr*, 2016. **27**(2): p. 71-8.
11. Lutt, W.W., in *Hepatic Circulation: Physiology and Pathophysiology*. 2009: San Rafael (CA).
12. James, J.L., P.R. Stone, and L.W. Chamley, *The effects of oxygen concentration and gestational age on extravillous trophoblast outgrowth in a human first trimester villous explant model*. *Hum Reprod*, 2006. **21**(10): p. 2699-705.
13. Ma, L.N., et al., *Lactic Acid: A Novel Signaling Molecule in Early Pregnancy?* *Front Immunol*, 2020. **11**: p. 279.
14. Mele, J., et al., *Impaired mitochondrial function in human placenta with increased maternal adiposity*. *Am J Physiol Endocrinol Metab*, 2014. **307**(5): p. E419-25.

15. Jarvie, E., et al., *Lipotoxicity in obese pregnancy and its potential role in adverse pregnancy outcome and obesity in the offspring*. Clin Sci (Lond), 2010. **119**(3): p. 123-9.
16. Scientific Animations. *3D Medical Illustration of Uterus*. 2020. [cited 2020]; Available from: <https://scientificanimations.com>.
17. Creative Commons. *Attribution-ShareAlike 4.0 International*. 2020. [cited 2020]; Available from: <https://creativecommons.org/licenses/by-sa/4.0/>.
18. National Institutes of Health. *What are some common complications of pregnancy?* 2017. [cited 2020]; Available from: <https://www.nichd.nih.gov/health/topics/pregnancy/conditioninfo/complications>.
19. Catalano, P.M. and K. Shankar, *Obesity and pregnancy: mechanisms of short term and long term adverse consequences for mother and child*. BMJ, 2017. **356**: p. j1.
20. Toro-Ramos, T., et al., *Body composition during fetal development and infancy through the age of 5 years*. Eur J Clin Nutr, 2015. **69**(12): p. 1279-89.
21. Fernandez-Twinn, D.S., et al., *Exercise rescues obese mothers' insulin sensitivity, placental hypoxia and male offspring insulin sensitivity*. Sci Rep, 2017. **7**: p. 44650.
22. Zanella, M.T., O. Kohlmann, Jr., and A.B. Ribeiro, *Treatment of obesity hypertension and diabetes syndrome*. Hypertension, 2001. **38**(3 Pt 2): p. 705-8.
23. Heydari, H., et al., *Maternal exposure to ambient air pollution during pregnancy and lipid profile in umbilical cord blood samples; a cross-sectional study*. Environ Pollut, 2020. **261**: p. 114195.
24. Wai, K.M., et al., *Protective role of selenium in the shortening of telomere length in newborns induced by in utero heavy metal exposure*. Environ Res, 2020. **183**: p. 109202.
25. Yee, L.M., et al., *Quality of periconceptional dietary intake and maternal and neonatal outcomes*. Am J Obstet Gynecol, 2020. **223**(1): p. 121 e1-121 e8.
26. Wilding, S., et al., *Are environmental area characteristics at birth associated with overweight and obesity in school-aged children? Findings from the SLOPE (Studying Lifecourse Obesity PrEdictors) population-based cohort in the south of England*. BMC Med, 2020. **18**(1): p. 43.
27. Mandy, M. and M. Nyirenda, *Developmental Origins of Health and Disease: the relevance to developing nations*. Int Health, 2018. **10**(2): p. 66-70.

28. Fall, C.H.D. and K. Kumaran, *Metabolic programming in early life in humans*. Philos Trans R Soc Lond B Biol Sci, 2019. **374**(1770): p. 20180123.
29. Musial, B., et al., *A Western-style obesogenic diet alters maternal metabolic physiology with consequences for fetal nutrient acquisition in mice*. J Physiol, 2017. **595**(14): p. 4875-4892.
30. Dashty, M., *A quick look at biochemistry: carbohydrate metabolism*. Clin Biochem, 2013. **46**(15): p. 1339-52.
31. Galgani, J. and E. Ravussin, *Energy metabolism, fuel selection and body weight regulation*. Int J Obes (Lond), 2008. **32 Suppl 7**: p. S109-19.
32. Zierhut, M.L., et al., *Kinetic modeling of hyperpolarized ¹³C1-pyruvate metabolism in normal rats and TRAMP mice*. J Magn Reson, 2010. **202**(1): p. 85-92.
33. Hillier, T.A., et al., *Childhood obesity and metabolic imprinting: the ongoing effects of maternal hyperglycemia*. Diabetes Care, 2007. **30**(9): p. 2287-92.
34. Ehrlich, S.F., et al., *Pregnancy glycemia in Mexican-American women without diabetes or gestational diabetes and programming for childhood obesity*. Am J Epidemiol, 2013. **177**(8): p. 768-75.
35. Kupinski, A.M., *Diagnostic Medical Sonography: The Vascular System*. Third Edition ed. 2013, Baltimore, MD: Lippincott Williams & Wilkins.
36. National Institutes of Health. *Type 2 diabetes*. 2020. [cited 2020]; Available from: <https://ghr.nlm.nih.gov/condition/type-2-diabetes>.
37. Canadian Liver Foundation. *Fatty Liver Disease*. 2017. [cited 2020]; Available from: <https://www.liver.ca/patients-caregivers/liver-diseases/fatty-liver-disease/>.
38. Obesity Canada. *What Causes Obesity?* [cited 2020]; Available from: <https://obesitycanada.ca/understanding-obesity/>.
39. Lloyd, L.J., S.C. Langley-Evans, and S. McMullen, *Childhood obesity and risk of the adult metabolic syndrome: a systematic review*. Int J Obes (Lond), 2012. **36**(1): p. 1-11.
40. Gunderson, E.P., *Childbearing and obesity in women: weight before, during, and after pregnancy*. Obstet Gynecol Clin North Am, 2009. **36**(2): p. 317-32, ix.
41. National Institutes of Health. *How Dietary Factors Influence Disease*. 2017. [cited 2020]; Available from: <https://www.nih.gov/news-events/nih-research-matters/how-dietary-factors-influence-disease-risk>.

42. Micha, R., et al., *Association Between Dietary Factors and Mortality From Heart Disease, Stroke, and Type 2 Diabetes in the United States*. JAMA, 2017. **317**(9): p. 912-924.
43. Office of Disease Prevention and Health Promotion. *Dietary Guidelines 2015-2020*. [cited 2020]; Available from: <https://health.gov/our-work/food-nutrition/2015-2020-dietary-guidelines/guidelines/chapter-2/current-eating-patterns-in-the-united-states/>.
44. Cordain, L., et al., *Origins and evolution of the Western diet: health implications for the 21st century*. Am J Clin Nutr, 2005. **81**(2): p. 341-54.
45. Sinclair, K.J., et al., *Quantification of fetal organ volume and fat deposition following in utero exposure to maternal Western Diet using MRI*. PLoS One, 2018. **13**(2): p. e0192900.
46. Sarr, O., et al., *The differential effects of low birth weight and Western diet consumption upon early life hepatic fibrosis development in guinea pig*. J Physiol, 2016. **594**(6): p. 1753-72.
47. Morrison, J.L., et al., *Guinea pig models for translation of the developmental origins of health and disease hypothesis into the clinic*. J Physiol, 2018. **596**(23): p. 5535-5569.
48. SOGC. *Your Pregnancy*. 2020. [cited 2020]; Available from: <https://www.pregnancyinfo.ca/your-pregnancy/>.
49. Sreetharan, S., et al., *Ionizing Radiation Exposure During Pregnancy: Effects on Postnatal Development and Life*. Radiat Res, 2017. **187**(6): p. 647-658.
50. Kremkau, F.W., *Sonography Principles and Instruments*. Eighth Edition ed. 2011, St.Louis, Missouri: Elsevier Saunders.
51. Carlin, A., et al., *The use of magnetic resonance imaging in the prediction of birthweight*. Prenat Diagn, 2020. **40**(1): p. 125-135.
52. Kadji, C., et al., *Magnetic resonance imaging for prenatal estimation of birthweight in pregnancy: review of available data, techniques, and future perspectives*. Am J Obstet Gynecol, 2019. **220**(5): p. 428-439.
53. Donald W. McRobbie, E.A.M., Martin J. Graves, Martin R. Prince, *MRI From Picture to Proton*. 2nd Edition ed. 2006, New York, USA: Cambridge University Press.
54. Sarracanie, M., et al., *Low-Cost High-Performance MRI*. Sci Rep, 2015. **5**: p. 15177.

55. Quinn, T.M., A.M. Hubbard, and N.S. Adzick, *Prenatal magnetic resonance imaging enhances fetal diagnosis*. J Pediatr Surg, 1998. **33**(4): p. 553-8.
56. Frates, M.C., et al., *Fetal anomalies: comparison of MR imaging and US for diagnosis*. Radiology, 2004. **232**(2): p. 398-404.
57. Meyer-Wittkopf, M., et al., *Evaluation of three-dimensional ultrasonography and magnetic resonance imaging in assessment of congenital heart anomalies in fetal cardiac specimens*. Ultrasound Obstet Gynecol, 1996. **8**(5): p. 303-8.
58. Tyler B. Coplen, Y.S., *Isotope-abundance variations and atomic weights of selected elements: 2016 (IUPAC Technical Report)*. Pure and Applied Chemistry, 2016. **88**(12): p. p. 1203-1224.
59. Lim, H., *A Longitudinal Study of Tumour Metabolism Using Hyperpolarized Carbon-13 Magnetic Resonance Spectroscopic Imaging in a Preclinical Model of Glioma*, in *Medical Biophysics*. 2017, The University of Western Ontario-Electronic Thesis and Dissertation Repository: London, ON, Canada.
60. Chung, B.T., et al., *First hyperpolarized [2-(13)C]pyruvate MR studies of human brain metabolism*. J Magn Reson, 2019. **309**: p. 106617.
61. Wiens, C.N., et al., *Chemical shift encoded imaging of hyperpolarized (13) C pyruvate*. Magn Reson Med, 2015. **74**(6): p. 1682-9.
62. Larson, P.E.Z., et al., *Investigation of analysis methods for hyperpolarized 13C-pyruvate metabolic MRI in prostate cancer patients*. NMR Biomed, 2018. **31**(11): p. e3997.
63. Hill, D.K., et al., *Model free approach to kinetic analysis of real-time hyperpolarized 13C magnetic resonance spectroscopy data*. PLoS One, 2013. **8**(9): p. e71996.
64. Heindel, J.J., et al., *Developmental Origins of Health and Disease: Integrating Environmental Influences*. Endocrinology, 2015. **156**(10): p. 3416-21.
65. Zheng, J., *Energy metabolism of cancer: Glycolysis versus oxidative phosphorylation (Review)*. Oncol Lett, 2012. **4**(6): p. 1151-1157.
66. Borengasser, S.J., et al., *In utero exposure to prepregnancy maternal obesity and postweaning high-fat diet impair regulators of mitochondrial dynamics in rat placenta and offspring*. Physiol Genomics, 2014. **46**(23): p. 841-50.
67. Friesen-Waldner, L.J., et al., *Hyperpolarized [1-(13) C]pyruvate MRI for noninvasive examination of placental metabolism and nutrient transport: A feasibility study in pregnant guinea pigs*. J Magn Reson Imaging, 2016. **43**(3): p. 750-5.

68. Granlund, K.L., et al., *Hyperpolarized MRI of Human Prostate Cancer Reveals Increased Lactate with Tumor Grade Driven by Monocarboxylate Transporter 1*. *Cell Metab*, 2020. **31**(1): p. 105-114 e3.
69. Smith, L.M., et al., *Optimizing SNR for multi-metabolite hyperpolarized carbon-13 MRI using a hybrid flip-angle scheme*. *Magn Reson Med*, 2020. **84**(3): p. 1510-1517.
70. R Core Team. *R: A language and environment for statistical computing*. 2013; Available from: <http://www.R-project.org/>.
71. 3D Slicer. *Slicer 4.10.2*. 2020; Available from: <https://www.slicer.org>.
72. Kikinis, R., Pieper, SD., Vosburgh, K. (2014). [3D Slicer: a platform for subject-specific image analysis, visualization, and clinical support](#). *Intraoperative Imaging Image-Guided Therapy*, Ferenc A. Jolesz, Editor 3(19):277–289 ISBN: 978-1-4614-7656-6 (Print) 978-1-4614-7657-3 (Online).
73. Kapur, Tina., Pieper, Steve., Fedorov, Andriy., Fillion-Robin, J-C., Halle, Michael., O'Donnell, Lauren., Lasso, Andras., Ungi, Tamas., Pinter, Csaba., Finet, Julien., Pujol, Sonia., Jagadeesan, Jayender., Tokuda, Junichi., Norton, Isaiah., Estepar, Raul San Jose., Gering, David., Aerts, Hugo J.W.L., Jakab, Marianna., Hata, Nobuhiko., Ibanez, Luiz., Blezek, Daniel., Miller, Jim., Aylward, Stephen., Grimson, W. Eric L., Fichtinger, Gabor., Wells, William M., Lorensen, William E., Schroeder, Will., Kikinis, Ron. 2016. ["Increasing the Impact of Medical Image Computing Using Community-Based Open-Access Hackathons: The NA-MIC and 3D Slicer Experience."](#) *Medical Image Analysis* 33 (October): 176–80.
74. Fedorov, A., Beichel, R., Kalpathy-Cramer, J., Finet, J., Fillion-Robin, J-C., Pujol, S., Bauer, C., Jennings, D., Fennessy, F.M., Sonka, M., Buatti, J., Aylward, S.R., Miller, J.V., Pieper, S., Kikinis, R. [3D Slicer as an Image Computing Platform for the Quantitative Imaging Network](#). *Magn Reson Imaging*. 2012 Nov;30(9):1323-41. PMID: 22770690. PMCID: PMC3466397.
75. MathWorks. *MATLAB*. 2020; Available from: <https://www.mathworks.com/help/index.html>.
76. Lazic, S.E. and L. Essioux, *Improving basic and translational science by accounting for litter-to-litter variation in animal models*. *BMC Neurosci*, 2013. **14**: p. 37.
77. Marceau, K., et al., *The Prenatal Environment in Twin Studies: A Review on Chorionicity*. *Behav Genet*, 2016. **46**(3): p. 286-303.
78. Rosenfeld, C.S., *Sex-Specific Placental Responses in Fetal Development*. *Endocrinology*, 2015. **156**(10): p. 3422-34.

79. Wiley, C.D. and J. Campisi, *From Ancient Pathways to Aging Cells-Connecting Metabolism and Cellular Senescence*. Cell Metab, 2016. **23**(6): p. 1013-1021.
80. Manna, S., C. McCarthy, and F.P. McCarthy, *Placental Ageing in Adverse Pregnancy Outcomes: Telomere Shortening, Cell Senescence, and Mitochondrial Dysfunction*. Oxid Med Cell Longev, 2019. **2019**: p. 3095383.
81. Moon, C.M., et al., *Metabolic biomarkers for non-alcoholic fatty liver disease induced by high-fat diet: In vivo magnetic resonance spectroscopy of hyperpolarized [1-(13)C] pyruvate*. Biochem Biophys Res Commun, 2017. **482**(1): p. 112-119.
82. Turer, A.T., et al., *Metabolomic profiling reveals distinct patterns of myocardial substrate use in humans with coronary artery disease or left ventricular dysfunction during surgical ischemia/reperfusion*. Circulation, 2009. **119**(13): p. 1736-46.
83. M.Kaur, A.J.H., Q. Chen, J.An, H. Rusinek, C. Nazzaro., E. Millan, M. Noz, E. Kramer, V.S. Lee, . *What Causes Diminished Corticomedullary Differentiation In Renal Insufficiency?* Proc. Intl. Soc. Mag. Reson. Med. 13 (2005) 2005; Available from: <https://cds.ismrm.org/ismrm-2005/Files/01917.pdf>.
84. Schroeder, K., et al., *Embryonic resorption in context to intragestational corpus luteum regression: a longitudinal ultrasonographic study in the European brown hare (*Lepus europaeus* PALLAS, 1778)*. Theriogenology, 2013. **80**(5): p. 479-86.

Appendices

Appendix 1: Permission for Figure 4.

ELSEVIER LICENSE
TERMS AND CONDITIONS
Jul 17, 2020

This Agreement between Mary-Ellen Empey ("You") and Elsevier ("Elsevier") consists of your license details and the terms and conditions provided by Elsevier and Copyright Clearance Center.

License Number	4850811375080
License date	Jun 16, 2020
Licensed Content Publisher	Elsevier
Licensed Content Publication	Journal of Magnetic Resonance
Licensed Content Title	Kinetic modeling of hyperpolarized ¹³ C1-pyruvate metabolism in normal rats and TRAMP mice
Licensed Content Author	Matthew L. Zierhut, Yi-Fen Yen, Albert P. Chen, Robert Bok, Mark J. Albers, Vickie Zhang, Jim Tropp, Ilwoo Park, Daniel B. Vigneron, John Kurhanewicz, Ralph E. Hurd, Sarah J. Nelson
Licensed Content Date	Jan 1, 2010
Licensed Content Volume	202
Licensed Content Issue	1
Licensed Content Pages	8
Start Page	85
End Page	92
Type of Use	reuse in a thesis/dissertation
Portion	figures/tables/illustrations
Number of figures/tables/illustrations	1
Format	both print and electronic
Are you the author of this Elsevier article?	No
Will you be translating?	No
Title	Quantifying Mid-pregnancy Placental Metabolism in Guinea Pigs Fed a Lifelong Western Diet
Institution name	University of Western Ontario
Expected presentation date	Aug 2020
Portions	Figure 1 Mary-Ellen Empey [REDACTED]
Requestor Location	[REDACTED]
Publisher Tax ID	Attn: Mary-Ellen Empey GB 494 6272 12
Total	0.00 CAD

Appendix 2: AUP Original Approval.



AUP Number: 2015-063
PI Name: Regnault, Timothy
AUP Title: Hyperpolarized 13c Mri Of Placental Metabolic Abnormalities Resulting From The Western Diet
Approval Date: 01/22/2016

Official Notice of Animal Use Subcommittee (AUS) Approval: Your new Animal Use Protocol (AUP) entitled "Hyperpolarized 13c Mri Of Placental Metabolic Abnormalities Resulting From The Western Diet" has been APPROVED by the Animal Use Subcommittee of the University Council on Animal Care. This approval, although valid for four years, and is subject to annual Protocol Renewal.2015-063::1

1. This AUP number must be indicated when ordering animals for this project.
2. Animals for other projects may not be ordered under this AUP number.
3. Purchases of animals other than through this system must be cleared through the ACVS office. Health certificates will be required.

The holder of this Animal Use Protocol is responsible to ensure that all associated safety components (biosafety, radiation safety, general laboratory safety) comply with institutional safety standards and have received all necessary approvals. Please consult directly with your institutional safety officers.

Submitted by: Copeman, Laura
 on behalf of the Animal Use Subcommittee
 University Council on Animal Care

Appendix 3: AUP Renewed Approval.



AUP Number: 2019-116
PI Name: Regnault, Timothy
AUP Title: Hyperpolarized 13C MRI of Placental Metabolic Abnormalities Resulting from the Western Diet
Approval Date: 02/01/2020

Official Notice of Animal Care Committee (ACC) Approval:
 Your new Animal Use Protocol (AUP) 2019-116:1: entitled "Hyperpolarized 13C MRI of Placental Metabolic Abnormalities Resulting from the Western Diet" has been APPROVED by the Animal Care Committee of the University Council on Animal Care. This approval, although valid for up to four years, is subject to annual Protocol Renewal.

Prior to commencing animal work, please review your AUP with your research team to ensure full understanding by everyone listed within this AUP.

As per your declaration within this approved AUP, you are obligated to ensure that:

- 1) Animals used in this research project will be cared for in alignment with:
 - a) Western's Senate MAPPs 7.12, 7.10, and 7.15
http://www.uwo.ca/univsec/policies_procedures/research.html
 - b) University Council on Animal Care Policies and related Animal Care Committee procedures
http://uwo.ca/research/services/animalethics/animal_care_and_use_policies.htm
- 2) As per UCAC's Animal Use Protocols Policy,
 - a) this AUP accurately represents intended animal use;
 - b) external approvals associated with this AUP, including permits and scientific/departmental peer approvals, are complete and accurate;
 - c) any divergence from this AUP will not be undertaken until the related Protocol Modification is approved by the ACC; and
 - d) AUP form submissions - Annual Protocol Renewals and Full AUP Renewals - will be submitted and attended to within timeframes outlined by the ACC.
 - e) http://uwo.ca/research/services/animalethics/animal_use_protocols.html
- 3) As per MAPP 7.10 all individuals listed within this AUP as having any hands-on animal contact will
 - a) be made familiar with and have direct access to this AUP;
 - b) complete all required CCAC mandatory training (training@uwo.ca); and
 - c) be overseen by me to ensure appropriate care and use of animals.
- 4) As per MAPP 7.15,
 - a) Practice will align with approved AUP elements;
 - b) Unrestricted access to all animal areas will be given to ACVS Veterinarians and ACC Leaders;
 - c) UCAC policies and related ACC procedures will be followed, including but not limited to:
 - i) Research Animal Procurement
 - ii) Animal Care and Use Records
 - iii) Sick Animal Response
 - iv) Continuing Care Visits
- 5) As per institutional OH&S policies, all individuals listed within this AUP who will be using or potentially exposed to hazardous materials will have completed in advance the appropriate institutional OH&S training, facility-level training, and reviewed related (M)SDS Sheets,
<http://www.uwo.ca/hr/learning/required/index.html>

Submitted by: Copeman, Laura
 on behalf of the Animal Care Committee
 University Council on Animal Care

Curriculum Vitae

Name: Mary-Ellen Empey

Post-secondary Education and Degrees:

B.MRS.
2014-2018
McMaster University
Hamilton, Ontario, Canada

M.Sc Candidate, Medical Biophysics
September 2018-present
The University of Western Ontario
London, Ontario, Canada

Honours Awards:

Western Graduate Research Scholarship
September 2018-August 2020

Related Work Experience:

Summer Research Assistant
The University of Western Ontario
May 2018-September 2018

Undergraduate Research Supervisor
The University of Western Ontario
September 2018-April 2020

Work-Study Student Supervisor
The University of Western Ontario
September 2018-April 2020

Community and Volunteer Activities:

2020/2 Seminar Chair, UWO- Medical Biophysics Department

2020/1 In-Utero MRI workshop Chair, Conference hosted by University of Oxford, UK

2019/4 Poster Judge, UWO- Medical Biophysics Department, A.C Burton and Undergraduate Research Day

2019/3 Registration Assistant, Imaging Network Ontario Conference

2019/2 Science Fair Judge, London Christian Academy

Presentation Contributions:

1. (2020). Increase in Mid-pregnancy Placental Pyruvate-to-Metabolite Conversion in Guinea Pigs Fed a Lifelong Western Diet. In-Utero MRI Workshop, Oxford, UK. 1st author.
2. (2020). Quantification of T1 & T2* Relaxation Times of Fetal Adipose Tissues & Fetal Muscle at 1.5T. In-Utero MRI Workshop, Oxford, UK. Co-author.
3. (2019). Increase in Mid-pregnancy Placental KPL in Guinea Pigs Fed a Lifelong Western Diet. University of Western Ontario, Medical Biophysics Seminars, London, Ontario, Canada. 1st author.
4. (2019). Quantification of T1 & T2* Relaxation Times of Fetal Tissues at 1.5T. London Imaging Discovery Day, London, Ontario, Canada. Co-author.
5. (2019). Quantification of T1 & T2* Relaxation Times of Fetal Tissues at 1.5T. Imaging Network Ontario, London, Ontario, Canada. Co-author.
6. (2019). Quantifying T1 and T2* Relaxation Times of Fetal Fat, Fetal Liver, Fetal Kidney, and Amniotic Fluid at 1.5T. International Society for Magnetic Resonance in Medicine 2019, Montreal, Quebec, Canada. Co-author.

Publications-

Journal Articles:

1. Simran Sethi, Stephanie A. Giza, Estee Goldberg, Mary-Ellen E. T. Empey, Sandrine de Ribaupierre, Genevieve D. Eastabrook, Barbra de Vrijer, Charles A. McKenzie. (2020). Quantification of T1 & T2* Relaxation Times of Fetal Tissues at 1.5T. Radiology. Submitted. Co-author.
2. Stephanie Giza, Simran Sethi, Lauren Smith, Mary-Ellen Empey, Lindsay Morris, Charles McKenzie. (2019). The Application of In-Utero Magnetic Resonance Imaging in

the study of Developmental Origins of Health and Disease. *Journal of Developmental Origins of Health and Disease*. Submitted. Co-author.

Conference Publications:

1. Simran Sethi, Stephanie Giza, Mary-Ellen Empey, Liz Lorusso, Barbra de Vrijer, Charles McKenzie. (2020). Quantification of T1 & T2* Relaxation Times of Fetal Adipose Tissues & Fetal Muscle at 1.5T. Wavelengths. Toronto, Ontario, Canada. Abstract. Co-author. Submitted.
2. Simran Sethi, Stephanie Giza, Mary-Ellen Empey, Barbra de Vrijer, Charles McKenzie. (2020). Quantification of T1 & T2* Relaxation Times of Fetal Adipose Tissues & Fetal Muscle at 1.5T. Imaging Network Ontario. Toronto, Ontario, Canada. Abstract. Co-author. Accepted.
3. Simran Sethi, Stephanie Giza, Mary-Ellen Empey, Barbra de Vrijer, Charles McKenzie. (2020). Quantification of T1 & T2* Relaxation Times of Fetal Adipose Tissues & Fetal Muscle at 1.5T. Imaging Network Ontario. Poster. Toronto, Ontario, Canada. Co-author. Accepted.
4. Mary-Ellen Empey, Lanette Friesen-Waldner, Lauren Smith, Lindsay Morris, Trevor Wade, Barbra de Vrijer, Timothy Regnault, Charles McKenzie. (2020). Increase in Mid-pregnancy Placental Pyruvate-to-Metabolite Conversion in Guinea Pigs Fed a Lifelong Western Diet. In-Utero MRI Workshop. Oxford, UK. Poster. 1st author. Accepted.
5. Simran Sethi, Stephanie Giza, Mary-Ellen Empey, Barbra de Vrijer, Charles McKenzie. (2020). Quantification of T1 & T2* Relaxation Times of Fetal Adipose Tissues & Fetal Muscle at 1.5T. In-Utero MRI Workshop. Oxford, UK. Poster. Co-author. Accepted.
6. Mary-Ellen Empey, Lanette Friesen-Waldner, Lauren Smith, Lindsay Morris, Trevor Wade, Barbra de Vrijer, Timothy Regnault, Charles McKenzie. (2020). Increase in Mid-pregnancy Placental Pyruvate-to-Metabolite Conversion in Guinea Pigs Fed a Lifelong Western Diet. In-Utero MRI Workshop. Oxford, UK. Abstract. 1st author. Accepted.
7. Simran Sethi, Stephanie Giza, Mary-Ellen Empey, Barbra de Vrijer, Charles McKenzie. (2020). Quantification of T1 & T2* Relaxation Times of Fetal Adipose Tissues & Fetal Muscle at 1.5T. In-Utero MRI Workshop. Oxford, UK. Abstract. Co-author. Accepted.
8. Mary-Ellen Empey, Lanette Friesen-Waldner, Lauren Smith, Cheryl Vander Tuin, Trevor Wade, Barbra de Vrijer, Timothy Regnault, Charles McKenzie. (2019). Increase in Mid-pregnancy Placental k_{PL} in Guinea Pigs Fed a Life-long Western Diet. *Southern Ontario Reproductive Biology*. Toronto, Ontario, Canada. Poster. 1st author. Accepted.
9. Simran Sethi, Stephanie Giza, Mary-Ellen Empey, Barbra de Vrijer, Charles McKenzie. (2019). London Imaging Discovery Day. London, Ontario, Canada. Abstract. Co-author. Accepted.

10. Mary-Ellen Empey, Lanette Friesen-Waldner, Lauren Smith, Trevor Wade, Barbra de Vrijer, Timothy Regnault, Charles McKenzie. (2019). London Imaging Discovery Day. London, Ontario, Canada. Abstract. 1st author. Accepted.
11. Mary-Ellen Empey, Lanette Friesen-Waldner, Lauren Smith, Cheryl Vander Tuin, Trevor Wade, Barbra de Vrijer, Timothy Regnault, Charles McKenzie. (2019). Increase in Mid-pregnancy Placental k_{PL} in Guinea Pigs Fed a Life-long Western Diet. Southern Ontario Reproductive Biology. Toronto, Ontario, Canada. Abstract. 1st author. Accepted.
12. Simran Sethi, Stephanie Giza, Mary-Ellen Empey, Barbra de Vrijer, Charles McKenzie. (2019). Quantifying T1 and T2* Relaxation Times of Fetal Fat, Fetal Liver, Fetal Kidney, and Amniotic Fluid at 1.5T. International Society of Magnetic Resonance in Medicine. Montreal, Quebec, Canada. Abstract. Co-author. Accepted.
13. Mary-Ellen Empey, Lanette Friesen-Waldner, Lauren Smith, Cheryl Vander Tuin, Trevor Wade, Barbra de Vrijer, Timothy Regnault, Charles McKenzie. (2019). Increase in Mid-pregnancy Placental k_{PL} in Guinea Pigs Fed a Life-long Western Diet. Child Health Research Day. London, Ontario, Canada. Poster. 1st author. Accepted.
14. Mary-Ellen Empey, Lanette Friesen-Waldner, Lauren Smith, Cheryl Vander Tuin, Trevor Wade, Barbra de Vrijer, Timothy Regnault, Charles McKenzie. (2019). Increase in Mid-pregnancy Placental k_{PL} in Guinea Pigs Fed a Life-long Western Diet. Child Health Research Day. London, Ontario, Canada. Abstract. 1st author. Accepted.
15. Simran Sethi, Stephanie Giza, Mary-Ellen Empey, Barbra de Vrijer, Charles McKenzie. (2019). Quantification of T1 & T2* Relaxation Times in Fetal Tissues at 1.5 Tesla. London Health Research Day. London, Ontario, Canada. Poster. Co-author. Accepted.
16. Mary-Ellen Empey, Lanette Friesen-Waldner, Lauren Smith, Cheryl Vander Tuin, Trevor Wade, Barbra de Vrijer, Timothy Regnault, Charles McKenzie. (2019). Imaging Placental Metabolism in Pregnant Guinea Pigs Fed a Western Diet. London Health Research Day. London, Ontario, Canada. Poster. 1st author. Accepted.
17. Simran Sethi, Stephanie Giza, Mary-Ellen Empey, Barbra de Vrijer, Charles McKenzie. (2019). Quantification of T1 & T2* Relaxation Times of Fetal Tissues at 1.5 Tesla. London Health Research Day. London, Ontario, Canada. Abstract. Co-author. Accepted.
18. Mary-Ellen Empey, Lanette Friesen-Waldner, Lauren Smith, Cheryl Vander Tuin, Trevor Wade, Barbra de Vrijer, Timothy Regnault, Charles McKenzie. (2019). Imaging Placental Metabolism in Pregnant Guinea Pigs Fed a Western Diet. London Health Research Day. London, Ontario, Canada. Abstract. 1st author. Accepted.
19. Simran Sethi, Stephanie Giza, Mary-Ellen Empey, Barbra de Vrijer, Charles McKenzie. (2019). Quantification of T1 & T2* Relaxation Times of Fetal Tissues at 1.5T. Imaging Network Ontario. London, Ontario, Canada. Abstract. Co-author. Accepted.